Journal of Materials Research and Technology 37 (2025) 2418–2433

Contents lists available at ScienceDirect

Journal of Materials Research and Technology

journal homepage: www.elsevier.com/locate/jmrt

A new Al80Mg10Si5Cu5 multicomponent aluminium alloy: Microstructure, mechanical, and physical properties

Ester Villanueva [a], Iban Vicario [a], Ignacio Crespo [a], Teresa Guraya [b], Iñaki Hurtado [c], Joseba Albizuri [b,*]

[a] Metal Processing Platform, TECNALIA, Basque Research and Technology Alliance (BRTA), Derio, E48160, Spain
[b] Faculty of Engineering of Bilbao, University of the Basque Country (UPV/EHU), Bilbao, E48013, Spain
[c] Mechanical and Manufacturing Department, Mondragon University, Arrasate-Mondragon, E20500, Spain

ARTICLE INFO

Keywords:
Aluminium
Multicomponent
HPDC process
Mechanical properties
Physical properties
High temperature

ABSTRACT

This study investigates the microstructure, mechanical, and physical properties of a newly developed and patented multicomponent aluminium alloy based on the AlMgSiCu system, produced by High Pressure Die casting (HPDC). This alloy exhibits superior mechanical properties compared to other HPDC alloys, especially at elevated temperatures. Tested at both room temperature (RT), and at 200 °C, a range where most aluminium alloys degrade, it demonstrated remarkable thermal stability, maintaining its characteristics. The alloy's complex microstructure includes an aluminium matrix with Mg_2Si, Al_2Cu, and Al_2CuMg phases. At 200 °C, the alloy's hardness was twice that of the commonly used AlSi9Cu3 alloy. The yield strength (YS) reached 244 MPa, ultimate tensile strength (UTS) 267 MPa, and elongation (E) of 0.69 %, showing a 65 % increase in YS and a 45 % increase in UTS, compared to AlSi9Cu3 alloy. In compressive testing, the alloy also showed superior results, with a YS of 251 MPa, ultimate compressive strength (UCS) of 468 MPa, and deformation (D) of 18.50 %, with a 90 % increase in YS and an 80 % increase in UCS. The results are significant, despite a 40 % lower deformation compared to AlSi9Cu3. The transformation of the Al_2Cu phase with temperature to form the Al_2CuMg phase had a significant impact on the material's overall mechanical properties, maintaining the mechanical properties at 200 °C. Comparing the YS, UTS and UCS-to-density ratio at 200 °C, this alloy shows great potential for high-temperature applications being an attractive candidate for aerospace and automotive sectors, particularly for components like drum brakes, traditionally made of cast iron.

1. Introduction

Aluminium alloys are important because of their potential for weight reduction in the transportation and energy industries, and because of other specific properties. Furthermore, the rise of electric vehicles is driving up the demand for aluminium alloys supported by the GIGA-PRESS technology by HPDC [1], and the study of its use for aluminium drum brakes [2,3].

Aluminium drum brakes are ideal for lightweight electric vehicles due to their lower rear braking forces compared to the front brakes. Kinetic Energy Recovery Systems (KERS) further decrease these forces, while front disc brakes engage before rear drum brakes, resulting in reduced pressure on the rear [4]. Aluminium drums are lighter than iron, providing better heat dissipation, reduced brake fade, and preventing corrosion and failure of conventional grey cast iron discs [5]. This is why several studies have proposed using aluminium-silicon (Al–Si) alloys or aluminium matrix composites reinforced with SiC [4].

Most commercial foundry alloys are based on the Al–Si system. The obtained microstructure is principally constituted by Al-dendrites [6]. Silicon (Si) plays an important role in increasing the castability of the alloy, and increasing strength values, but reducing machinability [7]. Automotive alloys typically contain Si between 5 wt% and 12 wt% [8]. Hypereutectic Al–Si alloys are employed for tribological applications. These alloys tend to have coarse primary Si precipitates, which increase hardness but reduce other mechanical properties such as ductility [9]. Magnesium (Mg) increases the strength and hardness of the alloy and makes the alloy heat-treatable [10] but can decrease the ductility. An insufficient Mg content leads to the formation of pure Si precipitates, which causes embrittlement in the alloy. Therefore, the Mg concentration is carefully adjusted to prevent the occurrence of free Si. At a Mg

* Corresponding author.
E-mail address: joseba.albizuri@ehu.eus (J. Albizuri).

https://doi.org/10.1016/j.jmrt.2025.06.171
Received 22 October 2024; Received in revised form 12 March 2025; Accepted 22 June 2025
Available online 23 June 2025

content of 1 % coarse primary silicon particles are evident, while increasing the Mg content to 6 % reduces the formation of Si particles and promotes the precipitation of primary Mg_2Si phases [11]. The Mg concentration directly influences the morphology and size of Mg_2Si precipitates, thereby affecting the alloy's ductility [12]. Additionally, copper (Cu) additions induce the formation of Al_2Cu precipitates, enhancing the alloy's hardness [13] with maximum strengthening achieved at copper concentrations between 4 wt% and 6 wt% [14]. Nevertheless, high copper content can decrease ductility and increase corrosion susceptibility [15]. The combined addition of copper and magnesium determines an increase of Cu and Mg-rich intermetallic with different morphologies [15]. In case of no more additional Si, the Al_2CuMg phase precipitates which is advantageous in aluminum alloys in comparison to Al_2Cu phase [16] due to its higher strength and hardness [17]. However, this phase can serve as a crack initiation source [18].

Aluminium conventional alloys have one dominant principal element (Al), and the quantities of other alloying elements are relatively small. Consequently, most casting alloys exhibit a limited combination of mechanical properties [19]. A current trend and new opportunity that has received significant research attention are the High Entropy Alloys (HEA), also called compositional complex alloys (CCAs) and multi-component alloys [20]. These alloys typically exhibit a higher entropy value compared to traditional aluminium alloys due to the addition of a larger quantity of secondary elements. The basic concept is to obtain a more disordered structure of five or more elements at or near an equi-molar composition, forming a solid solution phase [21]. The final crystalline structure plays a crucial role in the properties. When a pure FCC phase is formed, the alloy acts as a solid solution, exhibiting relatively low strength but high ductility. Pure BCC phases are extremely brittle. In a mixed-phase region, alloys performed as a composite, showing an increased strength [22]. The significant chemical differences and highly negative enthalpy between Al and the alloying elements often promote the formation of a substantial volume of intermetallic compounds (ICs). Several Al-based entropy alloys with exceptional properties have been reported [23]. The peculiarity of these new types of alloys lies in the significant improvement of their properties.

The manufacture of Light High Entropy Alloys (LWHEA) at a large scale remains limited [24,25], with vacuum arc melting as the main employed process [26]. In terms of tensile properties, the available data is very limited because these alloys tend to be brittle alloys with nearly no ductility [27]. As a result, most studies focus on the compressive properties of these alloys [28,29]. AlMgZnCu alloy showed UTS values of up to 450 MPa [30]. Al90Mg7.1Zn1.35Cu1.35Si0.3 alloy exhibited a YS of 198 MPa, an ultimate compressive strength (UCS) of 794 MPa, and a deformation (D) of 33 %. In contrast, the Al70Cu5Mg5Mn5Si10Zn5 alloy demonstrated a YS of 622 MPa, UCS of 644, and D of 2 % [31]. The Al40Cu15Cr15Fe15Si15, Al65Cu5Cr5Si15Mn5Ti5, and Al60Cu10-Fe10Cr5Mn5Ni5Mg5 alloys [32] showed the highest reported hardness-to-density ratio values, but with a fragile behaviour.

Within the foundry processes, HPDC offers a series of advantages, especially in the manufacturing of high volumes and low-cost structural and complex components [33]. Remarkably, this casting process represents about 60 % of all the aluminium castings employed in the automotive industry. HPDC process promotes a finer microstructure layer near the casting surface (surface layer or the skin), containing very fine dendritic primary aluminium grains [34] and improving mechanical properties [35]. In HPDC, the most widely used alloy is the AlSi9Cu3 (Fe) alloy, with a good combination of castability, properties, and price [36]. This alloy is commonly used in various automotive applications such as engine cylinder blocks, transmission housings, cylinder heads, and intake manifolds, due to its excellent balance of heat resistance and structural integrity properties. The obtained properties are essential for high-performance engine components [37].

These alloys contain around a 1 % wt. iron, promoting an easy release of the part from the die but reducing heat treatability [38], affecting its mechanical strength. Iron and silicon form intermetallics whose morphology impacts the feeding process, particularly in the presence of the needle-like β-Al_5FeSi phase. This phase is deleterious because it can serve potentially as a site for fractures [39]. The addition of manganese modifies the morphology of iron-rich phases from needle-like β-Fe phases to α-Fe phases, which appear in Chinese script or skeleton-like form, reducing the initiation of cracks. This transformation enhances both YS and UTS without compromising ductility [40]. These alloys combine high strength, adequate corrosion [15], and fatigue resistance [41].

The mechanical properties of aluminium alloys are affected at temperatures above 150 °C, resulting in the loss of hardness and mechanical properties [42–46]. The strengthening mechanisms of the alloy's microstructure become unstable, leading to the coarsening of intermetallic particles and a higher number of precipitates, which in turn softens the matrix [47]. AlSi9Cu3(Fe) alloys exhibited a reduction in hardness of around 25 % when exposed to temperatures above 100–150 °C [48] and also of UTS [49], due to the relaxation of residual stresses and the reduction of solute atoms, which diminishes the matrix strengthening.

Recent studies have investigated the production of HPDC multi-component alloys such as Al85Cu5Si5Zn5, Al65Cu10Mg10Si10Zn5 and Al80Cu5Mg5Si5Zn5 [50]. These alloys exhibited high YS and UCS under compressive forces, although they demonstrated minimal elongation at RT. Additionally, their mechanical properties decreased by more than 40 % at elevated temperatures [31]. Another HPDC alloy, AlCu-SiMgMnFe, exhibited a YS of 365 MPa and E of 1.8 % [51]. However, research on multicomponent alloys produced by HPDC, particularly for temperature applications, remains limited.

Rapid solidification processes improve the proportion of single-phase microstructures [52], minimizing the occurrence of large intermetallic phases [53], which are normally hard and fragile, and reducing their size. Regulating microstructural parameters can lead to substantial enhancements in mechanical properties [54], influenced by the cooling rate [55]. In HPDC, cooling rates are around 100 °C/s with an average SDAS size of less than 25 μm [56]. Thermal analysis (TA) can determine the cooling rate and characteristics of the solidification process [57–59]. The combination of TA with Factsage Software is a powerful tool for increasing the accuracy of results. While Factsage or Calphad are widely used in the design of aluminium alloys, it does have certain limitations [60] because they don't always accurately estimate the actual number of phases in multicomponent high entropy alloys [61] and the solidification characteristic temperatures.

In this research work, combined techniques were employed to design and validate the multiphase microstructure of a new semi-ductile as-cast multicomponent aluminium alloy based on the AlMgSiCu system produced by HPDC. The obtained microstructure was related to the mechanical and physical properties. The investigation showed the development of a new multicomponent aluminium alloy with enhanced properties such as strength at tensile and compressive forces, at RT and 200 °C, making it suitable for automotive drum applications. Unlike traditional cast iron drum brakes, aluminium matrix composite alloys are being explored as lightweight alternatives [62]. Aluminium drums significantly reduce vehicle weight, lowering unsprung and rotary mass, which improves handling and fuel efficiency. Additionally, aluminium's superior thermal conductivity enhances heat dissipation, reducing the risk of brake fade in high-temperature applications. Therefore, this new high-performance multicomponent aluminium alloy, produced via the HPDC process, presents a promising alternative for such applications. The working temperature of 200 °C was selected as a reasonably acceptable operating range for a drum brake under extreme conditions, such as mountain routes and successive braking actions. Higher values are considered excessive and more theoretical, particularly for aluminium brakes.

2. Materials and methods

2.1. Design of the new alloy

The design and development of the new alloy are based on previous research on 16 multi-component aluminium alloys, where various alloying elements were systematically adjusted and analyzed. These studies investigated different compositions derived from an AlMgSi matrix, incorporating Cu, Zn, Ca, Zr, Cr, and TiB in equiatomic proportions to enhance material properties.

As a result, the Al80Mg10Si5Cu5 alloy was selected as a promising candidate due to its high-temperature performance, wear resistance, and potential application in drum brakes, where similar properties are required [63].

2.2. Materials and samples preparation

Raw materials were melted, mixed, and held in a 500 Kg electrical furnace (Dugo EBC, Dugopa). The charge material for the new alloy consisted of recycled AlSi7Mg, AM60B, and AlSi9Cu3 alloys. Once the desired composition for the specific and selected alloy was achieved, the operating temperature was set to 700 °C, and the molten metal was injected into the metal die at 700 °C on a 950 t injection machine (PT-650, Pretansa). Additionally, an AlSi9Cu3 alloy was produced for comparative results because it is the most widely used in aluminium castings (around 60–70 %), and it's also manufactured by High-Pressure Die Casting (HPDC) [64].

The main HPDC manufacturing parameters are resumed in Table 1.

The chemical composition was determined by Inductively Coupled Plasma Optical Emission Spectrometer (ICP-OES) in a SPECTROMAXx (Spectro, RU) analyzer. Once solidified, the casting parts were extracted and submerged in water at 50 °C.

In Figs. 1 and 2 can be observed the equipment and the different casting parts obtained by HPDC.

2.3. Microstructure

2.3.1. Calphad method

To define the different solidified phases of the new alloy, FactSage version 8.3 (2023) was employed using the database FTlite (2023). This approach optimized the final microstructural composition of the alloy by examining the effects of each selected element in different proportions.

2.3.2. Thermal analysis

The application of TA enables determining the characteristic solidification temperatures, the number of precipitated phases, and their approximate percentages.

The cooling curve was analyzed using the recorded solidification temperature data. This data was collected with a high-speed National Instruments data acquisition system connected to a personal computer. Each TA trial was conducted at least three times. A custom-manufactured metal served as the die, achieving a cooling rate of about 5 °C/s.

Table 1
Main parameters of the HPDC casting for AlSi9Cu3 and Al80Mg10Si5Cu5.

Parameters	AlSi9Cu3	Al80Mg10Si5Cu5
Die temperature, °C	225	300
Alloy temperature, °C	680	700
Specific pressure, bar	800	800
Cycle time, s	57	57
1st plunger speed, m/s	0.4	0.4
2nd plunger speed, m/s	3.2	3.2

2.3.3. Optical and electrical microscope

Samples for metallographic evaluation were prepared using standard metallographic procedures. To ensure representative results, samples were extracted transversely from the neck area of the tensile test specimens.

The microstructure was evaluated using a Leica DMI5000 M (LEICA, Wetzlar, Germany) optical microscope (OM) and an EI Quanta 450 (FEI, Hills-boro, OR, USA) Scanning Electron Microscopy (SEM) equipped with Energy Dispersive Spectroscopy (EDX) for elemental analysis.

2.3.4. X-ray diffraction

X-ray diffraction (XRD) patterns and mineralogical information were obtained using a Philips X'Pert Pro MPD PW3040/60 X-ray diffractometer (Malvern Panalytical Ltd, United Kingdom), equipped with a copper anode operating with a voltage of 40 kV and 40 mA (1.6 kW). Scans were conducted over a 2θ range of 10°–90°, with a step size of 0.02° 2θ and each step lasting 2s. The XRD patterns were indexed using the PDF-2 database from the International Center for Diffraction Data (ICDD). XRD experiments were performed at RT and 200 °C.

2.4. Physical properties

2.4.1. Electric conductivity

Electric conductivity (EC) at RT was evaluated using a portable Autosigma 3000 conductivity meter. Conductivity measurements were taken from both the surface layer and the interior of the specimen.

2.4.2. Density

The density was determined using the Archimedean technique. A high-precision balance model BC Memory (Orma, Milan, Italy) with an accuracy of 0.01 mg was employed. After obtaining both dry and wet weight measurements, the following equation was applied to calculate the density of the new alloy:

$$\sigma_s = \frac{m_a}{m_a - m_l}\sigma_l \quad (1)$$

where m_l is the mass of the sample in the liquid (g), m_a is the mass of the sample in the air (g), σ_l is the density of the liquid (g/cm^3) and σ_s is the density of the solid (g/cm^3).

2.5. Mechanical properties

2.5.1. Hardness

Hardness at RT was evaluated using the Vickers test following the ISO 6507-1 ″ Standard for Metallic Materials [65]. The Vickers hardness was measured using an FV-700 model Vickers hardness tester with a load of 3 kgf.

The hardness tests at 200 °C were conducted using the Rockwell B scale with an EURO model tester, applying a 100 kgf load and a 2.5 mm diameter ball indenter. For these measurements, samples were heated and maintained at the testing temperature for about 50 min in a heating chamber (Instrom 3119-007). The obtained measures were then converted into Vickers hardness to compare the results with the hardness data at RT. It should be noted that these tests at 200 °C are not standardized. In both tests, ten measures were obtained from every sample.

2.5.2. Tensile strength

The tensile strength tests at RT were performed according to UNE EN ISO 6892-1 standard using an Instrom 5500R6025 device with a load range of 1–100 kN. The tests at 200 °C were performed following the UNE EN ISO 6892-2 standard. In this latter case, the process involved heating the samples from RT until the defined temperature for 30 min. Once the temperature was reached, the specimens were held at 200 °C for 15 min before the tensile tests were conducted. A heating chamber (Instrom 3119-007) was employed for the heating process. In both

Fig. 1. Detail of equipment HPDC machine and furnace.

Fig. 2. Example of tensile bars and other testing samples.

studies, a minimum of three tensile tests were performed.

2.5.3. Compression

The compression tests were conducted at RT and 200 °C. Cylindrical specimens with a diameter of 12 mm and a length of 20 mm were extracted and machined from the head area of the tensile test specimens. The employed equipment was the same as for the tensile tests and complied with the ASTM E−9 standard. A minimum of three specimens were employed for the evaluation.

3. Results

3.1. Microstructure

3.1.1. Chemical composition

ICP-OES was employed to determine the final chemical composition. Table 2 collects the chemical composition of Al80Mg10Si5Cu5 and AlSi9Cu3 alloys.

3.1.2. Calphad

The phase diagram of Al80Mg10Si5Cu5 alloy for equilibrium cooling conditions is depicted in Fig. 3, and under non-equilibrium conditions (Scheil approximation) in Fig. 4.

Simulation under equilibrium conditions predicted a significant proportion of FCC aluminium solid solution at temperatures ranging from 570 to 510 °C, along with the presence of the Mg_2Si phase. It can be observed that the Mg_2Si phase is precipitated before the aluminium nucleation point, forming primary Mg_2Si particles at 612 °C. In parallel to the aluminium precipitation, Mg2Si particles continue precipitating. As the cooling process progressed, around 509 °C, a second phase, S-Phase (Al_2CuMg) started precipitating, with a T-Al_2Cu phase precipitation at around 507 °C.

Under non-equilibrium conditions, the simulation predicted a significant proportion of the FCC aluminium solid solution at temperatures ranging from 582 to 500 °C, along with the presence of the Mg_2Si phase. It can be observed that the Mg_2Si phase is precipitated before the aluminium nucleation point, forming primary Mg_2Si particles at 612 °C. In parallel to the aluminium precipitation, Mg_2Si particles are created. As the cooling process progressed, around 510 °C, a second phase, T-Al_2Cu started precipitating, with a final S-Phase (Al_2CuMg) forming at around 507 °C.

Table 2
Elemental composition of Al80Mg10Si5Cu5 and AlSi9Cu3 alloys (wt.%).

Reference	Al	Mg	Si	Cu	Mn	Fe
Al80Mg10Si5Cu5	79.0	10.3	5.6	4.7	0.1	0.3
AlSi9Cu3	88.3	0.2	8.3	2.4	0.2	0.6

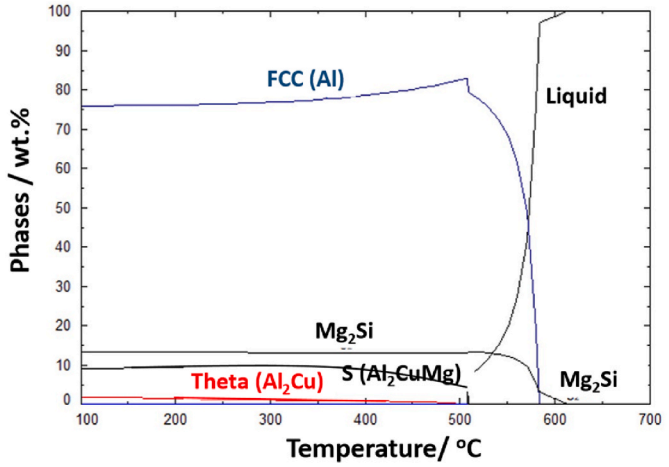

Fig. 3. Equilibrium diagram of Al80Mg10Si5Cu5 alloy.

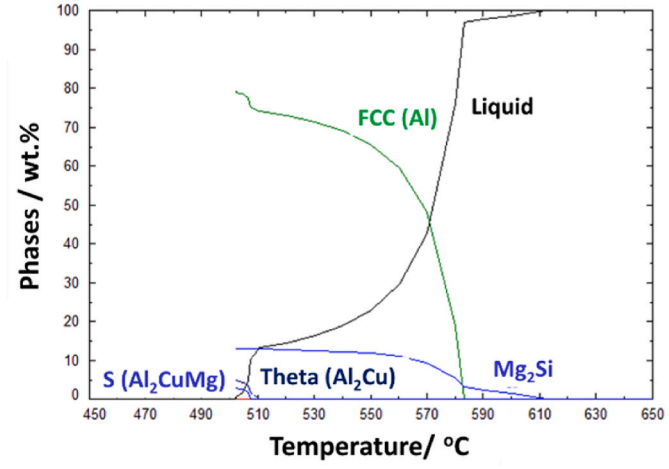

Fig. 4. Scheil phase diagram of Al80Mg10Si5Cu5 alloy.

It's remarkable in equilibrium and Scheil simulation that in a quite wide range of temperatures from 520 to 550 °C there is a zone where aluminium phase percentage is around 70 wt%, and there is only the presence of Mg_2Si which can allow the development of cooling and heat treatment processes to obtain a high saturated aluminium matrix or low and well distributed precipitated phases. In Scheil simulation, primary Si phase presence was not expected, which could decrease the ductility.

Table 3 summarizes the phases predicted by Factsage, along with the precipitation temperatures. In the equilibrium, the solidification range is between 612-507 °C, and in Scheil simulation is between 612-502 °C.

Remarkably, the total amount of Al_2Cu was slightly lower and Al_2CuMg slightly higher at equilibrium. However, the respective precipitation temperatures remained nearly unchanged, despite the difference in the order of phase precipitation.

Table 3
Max. percentage of every phase and temperatures at equilibrium (Equil.) and Scheil.

Phases	Max. wt.% Equil.	T range, °C Equil.	Max. wt.% Scheil	T range, °C Scheil
FCC-Al	82.86	583	79.14	583
Mg_2Si	13.36	612	12.96	612
S_phase-(Al_2CuMg)	9.37	509	4.79	507
Theta Al_2Cu	1.83	507	3.04	510

3.1.3. Thermal analysis

Table 4 summarizes the solidification temperatures obtained for correlated phases and Fig. 5 illustrates the cooling curve and the different correlated phases obtained by TA.

At the beginning of the curve, the precipitation of a pre-liquidus phase was determined, related in the literature with the presence of primary Mg_2Si [11,66]. This primary Mg_2Si has been predicted by the Factsage software. After the precipitation (nucleation and maximum point on the liquidus) corresponding to the FCC aluminium phase was detected. Subsequently, the precipitation of a third phase (nucleation and maximum on the eutectic) corresponding to the eutectic Al + Mg_2Si phase was observed [67]. Towards the end of the cooling curve and before reaching the solidus point, the post-eutectic Theta-phase Al_2Cu phase precipitated, followed by the precipitation of the S-phase Al_2CuMg, which presents a lower melting point than Al_2Cu phase [68]. In this latter case, the phase exhibited recalescence, indicating different values for the minimum and the maximum point on the post-eutectic phase [69]. The final sequence of precipitation has been correlated by the microstructure analysis.

The obtained data were compared with the Scheil simulation results for the predicted phases and solidification sequences, revealing slight differences in the predicted solidification temperatures, with deviations of around 10–20 °C, that can be correlated with the approx. 5 °C/s cooling rate obtained in the TA test.

To corroborate and validate the obtained data, the microstructure was analyzed by XRD, optical, and electrical microscope.

3.1.4. XRD at room temperature and 200 °C

XRD was employed to study the different phases, and the results can be observed in Fig. 6. The as-cast Al80Mg10Si5Cu5 alloy presented an aluminium matrix with Mg_2Si, Al_2CuMg, and Al_2Cu phases.

In Fig. 7, it can be observed the obtained results at 200 °C. As the test temperature increased, the Al_2Cu phase disappeared, becoming the Al_2CuMg phase. There is a slight decrease in the aluminium percentage in the FCC aluminium matrix in the samples tested at 200 °C, shown by the lowest intensity counts values. It has been observed that lower intensity counts values of the Mg_2Si phases were related with the partial dissolution of the Mg_2Si phase into the matrix. In the case of the Al_2CuMg phase, it does not appear to be dissolved into the matrix at these temperatures, maintaining a similar XRD values and characteristic points.

3.1.5. Optical and electrical microscope at RT and 200 °C

Figs. 8 and 9 show the optical microscope (OM) images of the Al80Mg10Si5Cu5 alloy tested at RT and 200 °C, respectively. A distinct difference between the surface layer and the interior area of the sample was observed, which is characteristic of the HPDC process.

According to FactSage calculations, Mg_2Si phases precipitated before aluminium, and in the microstructure, primary Mg_2Si particles were observed, corroborating calculations. This indicates that a Mg/Si ratio of 1.83 can facilitate the precipitation of primary Mg_2Si phases, whereas

Table 4
TA correlated characteristic phases and solidification temperatures.

Solidification parameters	T^a
T^a nucleation pre-liquidus (Mg_2Si)	592.0 °C
T^a nucleation liquidus (FCC–Al)	582.0 °C
T^a maximum on the liquidus (FCC–Al)	579.9 °C
T^a nucleation eutectic (FCC + Mg_2Si)	574.8 °C
T^a maximum on the eutectic (FCC + Mg_2Si)	570.7 °C
T^a nucleation post-eutectic[1] Al_2Cu	495.8 °C
T^a maximum on the post-eutectic[1] Al_2Cu	490.8 °C
T^a nucleation post-eutectic[2] Al_2CuMg	488.8 °C
T^a minimum on the post-eutectic[2] Al_2CuMg	487.6 °C
T^a maximum on the post-eutectic[2] Al_2CuMg	491.8 °C
T^a solidus	482.2 °C

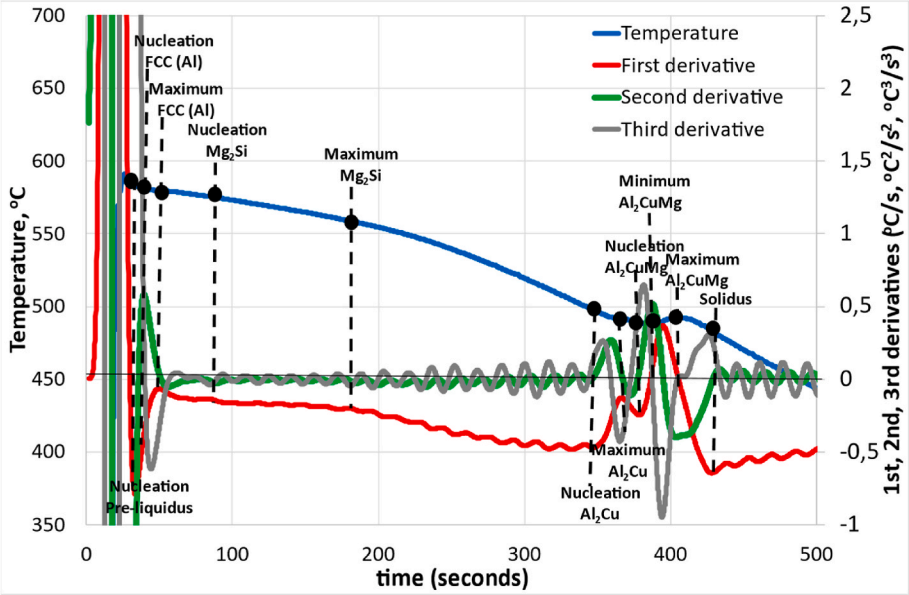

Fig. 5. Detail of cooling curve and first, second, and third derivative curves.

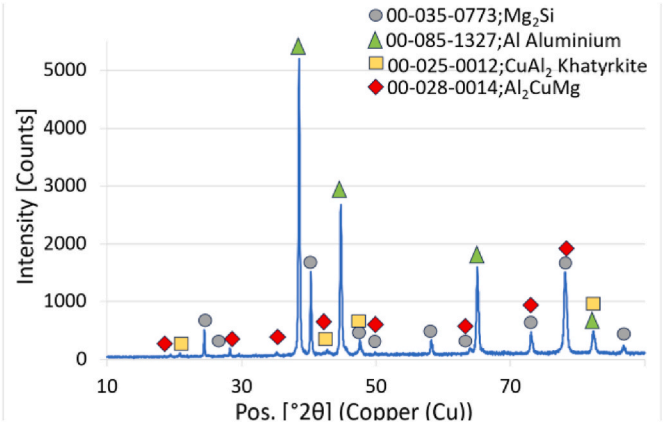

Fig. 6. XRD analysis at RT.

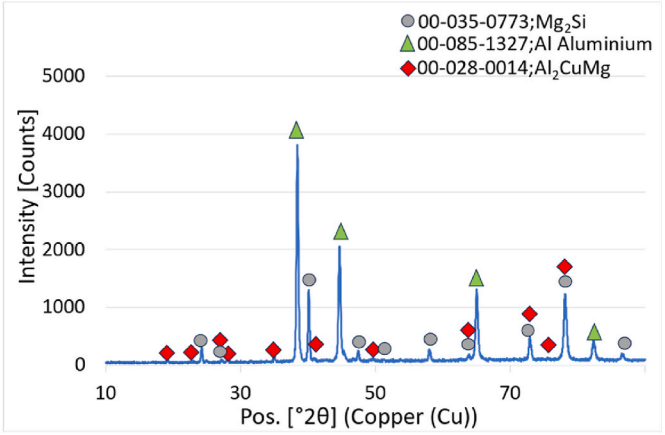

Fig. 7. XRD analysis at 200 °C.

higher Mg/Si ratios may favour the formation of eutectic or secondary phases, as demonstrated in previous studies [70]. These primary Mg_2Si particles were significantly larger than eutectic Mg_2Si particles, as shown in the figures. Also, the morphology of primary Mg_2Si presented generally a polyhedral plate morphology [71]. In contrast, eutectic Mg_2Si generally presented a fine lamellar morphology, related with the high cooling rates of HPDC process and the composition of the alloy.

Fig. 10 presents SEM images at RT, while Table 5 shows the chemical composition of the principal components. It is noted that the EDS spot included the surrounding areas of the analyzed phases, so the obtained composition must be taken as approximate. However, despite this, by comparing the chemical composition with various sources in the literature [72,73], the Mg_2Si, Al_2Cu, and Al_2CuMg phases detected in the XRD analysis were correlated with the SEM images.

Five different points of different areas and precipitates were studied. A predominant grey region (point A in yellow colour) aluminium matrix area with dendritic morphology was identified. Point B and point C comprised primary and eutectic Mg_2Si phases, which appeared as dark regions. Point D and point E (in orange and purple colour) consisted of copper-rich interdendritic intermetallics, corresponding to the Al_2Cu and Al_2CuMg phases, which appeared as the lighter regions.

Interdendritic copper phases were smaller in the skin or superficial area. The size of the primary phases of Mg_2Si in the interior was slightly larger than in the skin, reaching sizes from around 21 ± 7.97 μm, in comparison with 14 ± 7.85 μm in the skin area, and the amount of this intermetallic was smaller in the skin area. On the other hand, the eutectic Mg_2Si phases, which were smaller than the primary Mg_2Si phase (4.2 ± 1.46 μm large in the interior), are more visible in the interior [34].

No iron phases were detected, likely due to their small size promoted by the high cooling rates of the HPDC process, where typical intermetallics phases range from 10 to 50 μm [74]. The absence of β-iron phases prevents their detrimental effect on the alloy's mechanical properties.

Fig. 11 presents the elemental mapping at RT. Mg and Cu were homogeneously distributed in the Al matrix, but Si was not observed, probably due to the low amount of dissolved Si in the Al matrix. In the primary Mg_2Si phase, only Si and Mg were observed. In eutectic Mg_2Si, some Al was detected, which was correlated with the eutectic microstructure, a mixture of Al matrix and Mg_2Si precipitates. In the Al_2Cu phase, only Al and Cu were detected, with some Mg in the Al_2CuMg phase. It can be observed that Mg has a higher affinity with Si than Cu.

Fig. 12 shows SEM images at 200 °C, while Table 6 presents the approximative chemical composition of the phases. Four different points

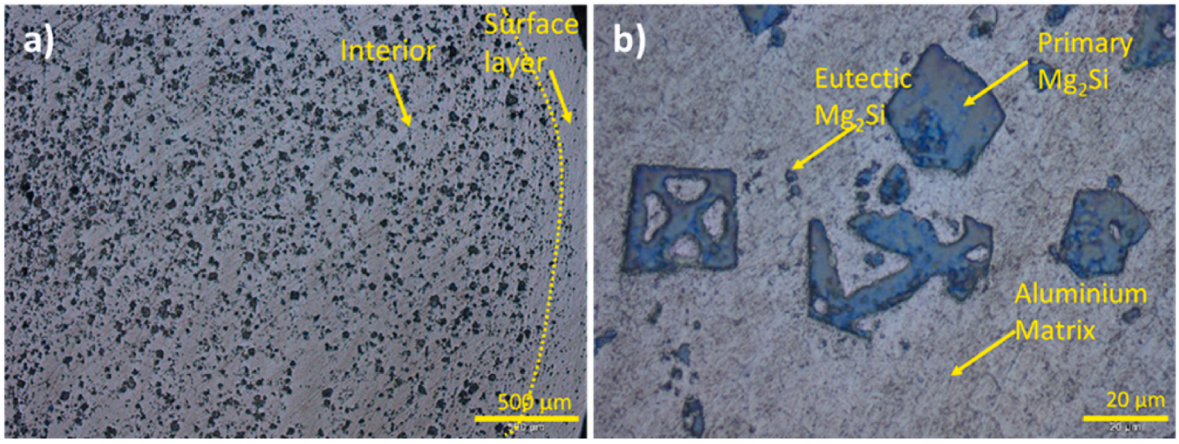

Fig. 8. OM of the as-cast Al80Mg10Si5Cu5 at RT: a) x50, b) x1000 augmentations.

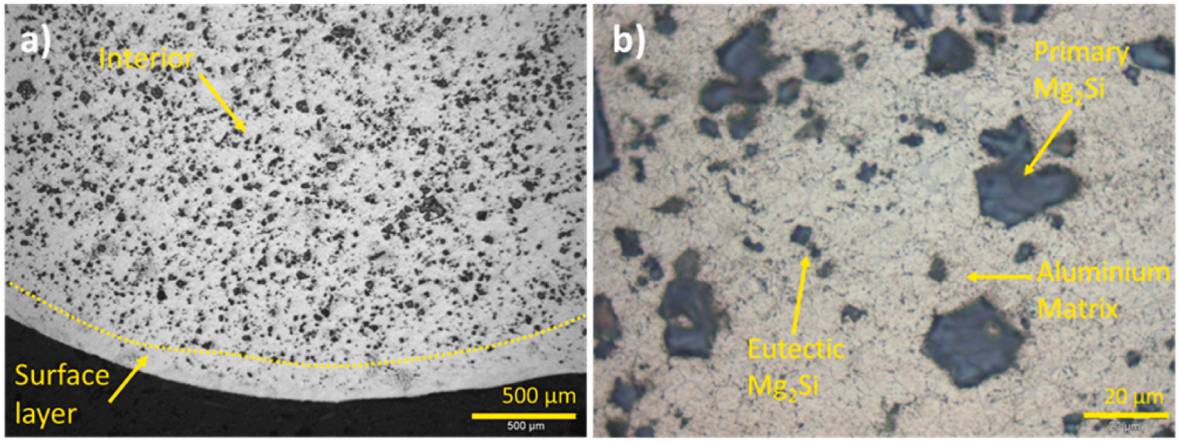

Fig. 9. OM of the as-cast Al80Mg10Si5Cu5 at 200 °C: a) x50, b) x1000 augmentations.

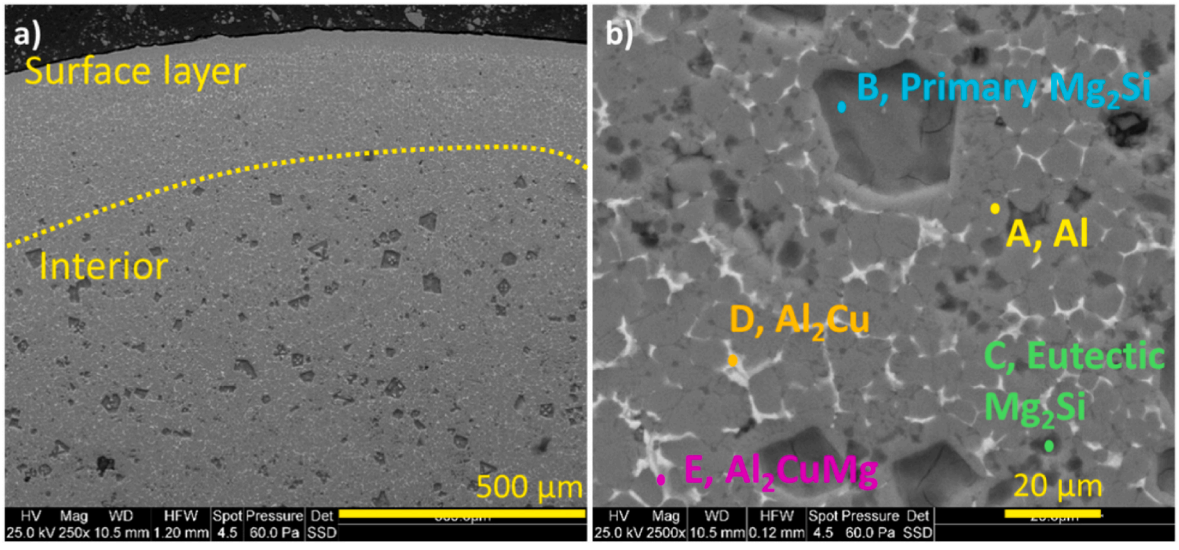

Fig. 10. SEM of the as-cast Al80Mg10Si5Cu5 at RT: a) x250, b) x2500 augmentations.

were identified, and the phases detected in the XRD analysis were correlated with the SEM images.

Some primary particles reached sizes of approximately 42,13 ± 13.89 µm, although most were very similar in size to those observed at RT. The eutectic Mg_2Si particles remained stable in size.

Table 5
Elemental composition (wt.%) of the analyzed points and correlation with XRD phases at RT.

Point	Phase	Al	Mg	Si	Cu
A	Al	88.49	6.78	1.98	2.75
B	Primary Mg_2Si	42.32	29.76	24.97	2.95
C	Eutectic Mg_2Si	66.89	16.90	13.60	2.62
D	Al_2Cu	66.27	8.37	1.31	24.05
E	Al_2CuMg	75.60	10.64	2.06	11.70

3.2. Physical properties

3.2.1. Electric conductivity

The results of electrical conductivity measurements in the different areas of the experimental alloys are presented in Table 7. The conductivity in the surface layer was slightly higher than in the interior. This is due to the reported differences in the microstructure between the surface and internal areas in HPDC process [75].

In the internal area, there was a more pronounced presence of Mg_2Si phases, which is known to decrease electrical conductivity. In contrast, the surface layer exhibited higher conductivity due to a higher concentration of Mg in solid solution, which is the main factor in increasing thermal conductivity [76]. This phenomenon is attributed to the faster cooling rate in the surface layer, which results in a greater amount of Mg retained in the Al matrix as a solid solution.

In comparison, pure aluminium is one of the most conductive materials with an electrical conductivity value of 63 % IACS [77]. Aluminium alloys typically exhibit electrical conductivity values ranging between 21 and 33 % IACS [78,79]. Measurements on the

Table 6
Elemental composition (wt.%) of the analyzed points and correlation with XRD phases for samples tested at 200 °C.

Region	Phase	Al	Mg	Si	Cu
F	Al	87.53	7.12	2.23	3.12
G	Primary Mg_2Si	41.27	31.32	23.12	4.29
H	Eutectic Mg_2Si	65.93	18.20	14.12	1.75
I	Al_2CuMg	72.30	11.55	1.96	13.29

Table 7
Electrical conductivity of Al80Mg10Si5Cu5 and AlSi9Cu3 alloys.

Reference	EC (%IACS)
Al80Mg10Si5Cu5 surface layer	21.0 ± 0.29
Al80Mg10Si5Cu5 interior	17.0 ± 0.55
AlSi9Cu3 surface layer	28.7 ± 0.30
AlSi9Cu3 interior	22.9 ± 0.28

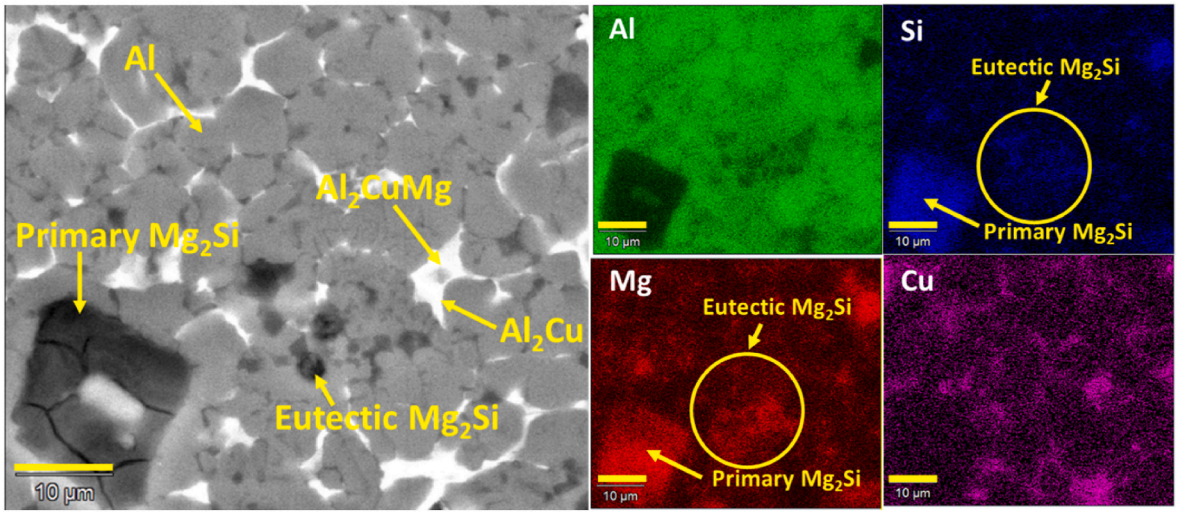

Fig. 11. SEM + EDS elemental mapping of the as-cast Al80Mg10Si5Cu5 at RT x 5000 augmentation.

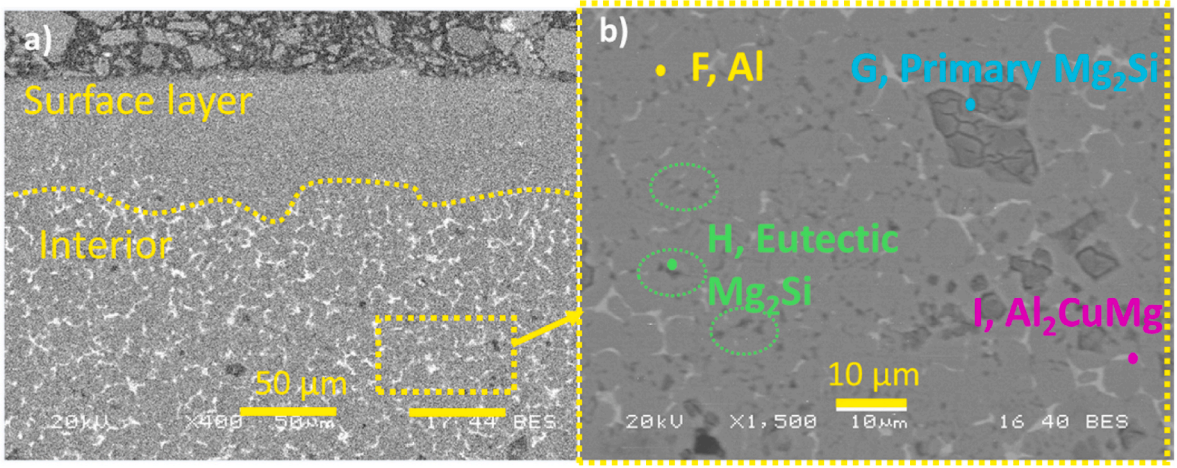

Fig. 12. SEM of the as-cast Al80Mg10Si5Cu5 at 200 °C: a) x400, b) x1500 augmentations.

experimental AlSi9Cu3 alloy confirmed these ranges.

When comparing these values with those obtained for the experimental Al80Mg10Si5Cu5, the results indicated that it had similar electrical conductivity to standard foundry alloys, with a slight decrease of around 25 % compared to the experimental AlSi9Cu3.

3.2.2. Density

Density results are presented in Table 8. Compared to previous lightweight multi-component aluminium alloys manufactured by HPDC, the achieved values were well below the reported values [28]. The selection of the alloying elements and their percentage produced a new alloy around 10 % lighter than the AlSi9Cu3 alloy used as the base for comparison.

3.3. Mechanical properties

3.3.1. Hardness

Table 9 shows the hardness values of the Al80Mg10Si5Cu5 and AlSi9Cu3 alloy tested at RT and 200 °C.

The Al80Mg10Si5Cu5 alloy exhibited an increase in hardness of about 40 % compared to the AlSi9Cu3 alloy, whose hardness values were similar to those reported in the literature [48].

At 200 °C hardness values decreased only by less than 8 % in Al80Mg10Si5Cu5 alloy, being very similar to those at RT.

3.3.2. Tensile strength

The tensile engineering properties, YS, UTS, and E, for the Al80Mg10Si5Cu5 alloy and AlSi9Cu3 at RT and 200 °C are shown in Table 10 and Fig. 13.

Despite the limited elongation in absolute terms of the Al80Mg10Si5Cu5 alloy, the UTS at RT was comparable to that of AlSi9Cu3 alloys aligning with the values reported for commercial AlSi9Cu3 alloys [80–82]. Additionally, the YS of Al80Mg10Si5Cu5 was 15 % higher than that of AlSi9Cu3 alloy.

At 200 °C, the Al80Mg10Si5Cu5 alloy exhibited UTS approximately 25 % higher than that of the AlSi9Cu3 alloy, with YS surpassing AlSi9Cu3 by 40 %, also exceeding the values observed at RT.

Fig. 14 shows the SEM analysis of the fracture surfaces of the Al80Mg10Si5Cu5 alloy after tensile testing at RT and 200 °C, revealing that cracks were predominantly initiated within the matrix.

At RT and 200 °C, the fracture surface exhibited cleavage facets in the harder primary Mg_2Si phases. The surfaces also displayed irregular morphologies with a fibrous appearance, featuring tear ridges and dimples, indicative of energy absorption and plastic deformation provided by the aluminium matrix before fracture [83–86].

The presence of some dendrites was remarkable and confirmed the presence of some shrinkage porosity in the studied samples.

Some minor cracks initiated in the porosity area were observed, with propagation along the interdendritic areas and eventually interconnected. In some cases, cracks traversed eutectic Mg_2Si particles, resulting in a transgranular fracture [87].

3.3.3. Compressive strength

The compressive engineering properties YS, Ultimate Compressive Strength (UCS), and Deformation (D) for the new as-cast Al80Mg10Si5Cu5 alloy and AlSi9Cu3 at RT and 200 °C are shown in Table 11 and Fig. 15.

The Al80Mg10Si5Cu5 alloy exhibited a high strength, with fracture strength exceeding 500 MPa at RT.

Compared to AlSi9Cu3, both the yield strength and maximum load were significantly higher, exhibiting increases of 40 % and 25 %, respectively, while the deformation was lower. The high deformation in AlSi9Cu3 may be attributed to its lower hardness.

At 200 °C, the UCS of the Al80Mg10Si5Cu5 alloy decreased by only about 12 %, while the values YS and D increased by 106 % and 166 %, indicating an enhancement in ductility.

In the case of AlSi9Cu3, the degradation in mechanical properties was substantial at 200 °C, particularly in terms of the UCS, which experienced a reduction of 40 %.

Otherwise, the ultimate compressive strength values at 200 °C for the Al80Mg10Si5Cu5 alloy were superior to those of other comparable alloys, such as AlSi7Mg, AlSiMgCu and AlSi9Cu3 produced by conventional process [41,88,89].

Fig. 16 shows the images of the specimen's fracture of Al80Mg10Si5Cu5 and AlSi9Cu3 alloy after the compressive test at RT and 200 °C. In the Al80Mg10Si5Cu5 alloy at RT, the fracture propagation started at a 45-degree angle to the loading direction of compression, but at a certain area of the specimen, the crack impacted on another crack or some defect of the material, forming a final vertical crack, and finally a catastrophic brittle fracture occurred [90].

In the case of the specimen of the Al80Mg10Si5Cu5 alloy at 200 °C, the fracture also propagated at a 45-degree angle but involved a considerable plastic deformation of the sample before the fracture.

Finally, Fig. 17 shows the SEM analysis of the fracture surfaces of the as-cast Al80Mg10Si5Cu5 alloy after compressive testing at RT and 200 °C.

The fracture surface at RT exhibited ductile elongated dimples with some cleavage facets in the primary Mg_2Si particles. Secondary cracks were visible in the primary Mg_2Si particles. Also, some dendrite characteristics of shrinkage defects were visible. At 200 °C the fracture surface was covered with numerous shear lips and no cracks were visible. This indicates that the Al80Mg10Si5Cu5 alloy was much more plastically deformed before reaching the final fracture [91].

Table 8
Results of the density of new as-cast multicomponent Al80Mg10Si5Cu5 and AlSi9Cu3 alloy.

Reference	σ_s (g/cm^3)
Al80Mg10Si5Cu5	2.58 ± 0.01
AlSi9Cu3	2.73 ± 0.04

Table 9
HV3 values of Al80Mg10Si5Cu5 and AlSi9Cu3 alloy tested at RT and 200 °C.

Reference	HV3
Al80Mg10Si5Cu5 - RT	136 ± 5.0
AlSi9Cu3 - RT	96 ± 7.3
Al80Mg10Si5Cu5 - 200 °C	126 ± 4.1
AlSi9Cu3 - 200 °C	68 ± 3.8

Table 10
Tensile test values of Al80Mg10Si5Cu5 and AlSi9Cu3 alloy tested at RT and 200 °C.

Temperature	YS (MPa)	UTS (MPa)	E (%)
Al80Mg10Si5Cu5 at RT	212 ± 19.5	258 ± 5.4	0.64 ± 0.3
AlSi9Cu3 at RT	180 ± 7.7	257 ± 13.7	2.92 ± 0.8
Al80Mg10Si5Cu5 at 200 °C	244 ± 38.3	267 ± 10.4	0.69 ± 0.2
AlSi9Cu3 at 200 °C	145 ± 20.1	182 ± 12.8	3.97 ± 2.1

4. Discussion

4.1. Validation of the model and methodology

According to the simulation, the cooling rate not only affects the precipitation temperatures but also affects the phase formation sequence, especially the copper phases. In this case, the high cooling rates inherent in the HPDC process are consistent with the phases estimated by the Scheil simulation, which align with the results obtained from the thermal analysis, with slight variations in solidification

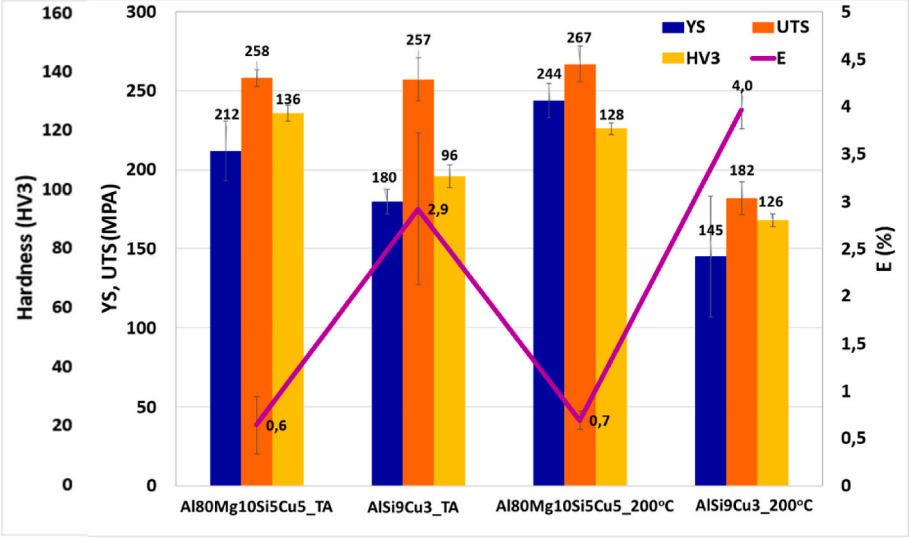

Fig. 13. Graphical display of mechanical properties (Hardness, Yield Strength, Ultimate Tensile Strength and Elongation).

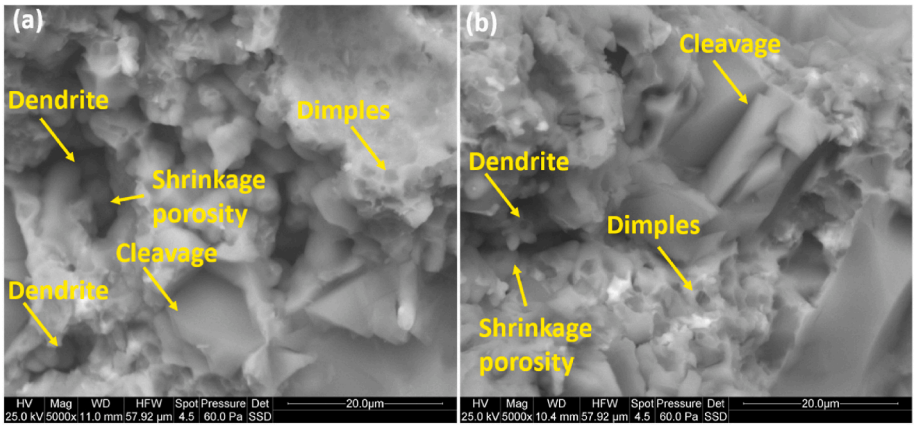

Fig. 14. (a) x5000 SEM of tensile test specimens of Al80Mg10Si5Cu5 alloy (a) at RT, (b) at 200 °C.

Table 11
Compressive test values of the Al80Mg10Si5Cu5 and AlSi9Cu3 alloy at RT and 200 °C.

Reference	YS (MPa)	UCS (MPa)	D (%)
Al80Mg10Si5Cu5 - RT	235 ± 7.0	531 ± 43.3	11.10 ± 2.3
AlSi9Cu3 -RT	138 ± 8.4	428 ± 9.9	23.33 ± 4.6
Al80Mg10Si5Cu5 -200 °C	251 ± 8.5	468 ± 34.1	18.50 ± 3.9
AlSi9Cu3 – 200 °C	132 ± 15.0	258 ± 10.0	30.83 ± 3.3

temperatures. These results suggest that the experimental conditions closely resemble this behaviour, validating the applicability of the model in describing the solidification sequence of the alloy under rapid cooling conditions. The employment of thermal analysis is a useful tool for validating the phase prediction and determining the phase formation temperatures.

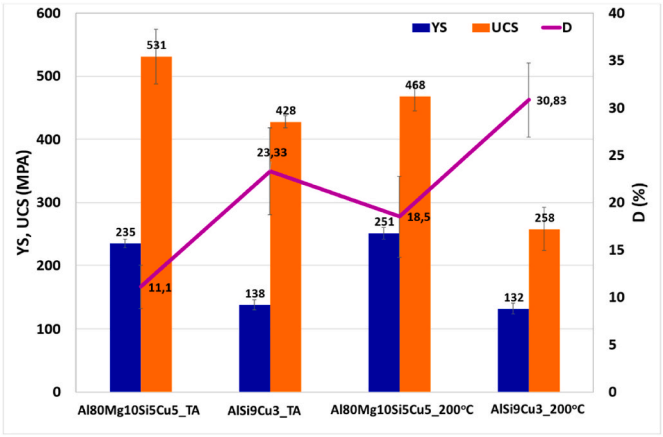

Fig. 15. Graphical display of mechanical properties (Yield Strength, Ultimate Compressive Strength and Deformation).

4.2. Phase transformation with temperature

The transformation of Al_2Cu into Al_2CuMg at 200 °C agrees with previous studies, which indicate that Al_2Cu is metastable and transforms into Al_2CuMg upon thermal exposure. This is consistent with the XRD results, where Al_2CuMg remained stable while Al_2Cu disappeared. The decrease in intensity of the Mg_2Si phase suggests partial dissolution into the Al matrix, which is expected due to the solubility of Mg and Si in Al at elevated temperatures.

The findings referring to the temperature range and phase distribution observed in the simulations and thermal analysis, suggest that

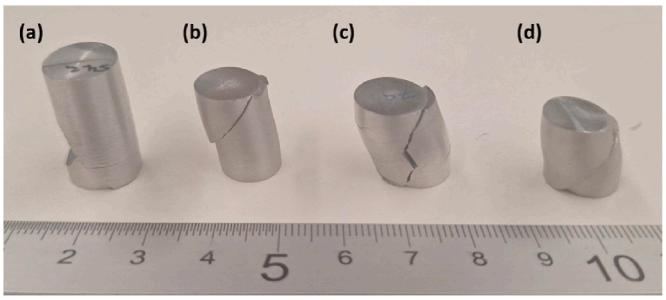

Fig. 16. Specimen's fracture under compressive of a) Al80Mg10Si5Cu5 at RT, b) AlSi9Cu3 at RT, c) Al80Mg10Si5Cu5 at 200 °C, d) AlSi9Cu3 at 200 °C.

specific cooling and heat treatment processes could be developed to achieve a highly saturated aluminium matrix or a well-distributed precipitation of phases. This led to better values of elongation in the new multicomponent HPDC alloy.

4.3. The effect of the microstructure

The observed difference between the surface and interior microstructure is characteristic of the HPDC process. The presence of large polyhedral primary Mg_2Si particles, along with finer eutectic Mg_2Si, ensures a balance between strength and ductility. The eutectic Mg_2Si, with its fine lamellar morphology, improves ductility by reducing stress concentration in the matrix, whereas the primary Mg_2Si contributes to hardness and wear resistance. The precipitation of Mg_2Si phases before Al aligns with Factsage.

This supports the hypothesis that an Mg/Si ratio of 1.83 favours the formation of primary Mg_2Si [70]. Additionally, the absence of β-iron phases is beneficial, as their presence is typically detrimental to mechanical properties. The high cooling rates in HPDC likely prevented the formation of these phases, as reported in similar studies [92].

The presence of interdendritic copper intermetallics in the interior and their reduced size in the skin suggests a correlation with solidification conditions.

At 200 °C, the increase in the number of Cu-rich intermetallics on the surface can be attributed to the accelerated diffusion of Cu atoms to the surface, combined with the precipitation of Cu from the over-saturated Al matrix [93]. This is supported by the elemental mapping results, which showed an increased presence of Cu-rich phases at higher temperatures.

Regarding Mg_2Si particles, their slight growth at 200 °C can be explained by the coalescence of precipitates and the precipitation of Si and Mg from the over-saturated matrix. However, the overall stability in size suggests that these particles do not significantly dissolve at this temperature, maintaining their strengthening effect on the alloy.

4.4. Physical properties

4.4.1. Electrical conductivity

The observed variation in electrical conductivity between the surface and interior is consistent with previous studies on HPDC alloys. The higher conductivity in the surface layer can be attributed to the lower volume fraction of Mg_2Si precipitates and the higher concentration of Mg in solid solution. The increased presence of precipitates in the interior acts as scattering centers for electrons, reducing conductivity.

These results support the well-established correlation between microstructure and electrical properties: an increase in the amount and size of precipitate phases decreases electrical conductivity [94].

This aligns with the fact that solid solution strengthening typically enhances conductivity when solute elements such as Mg remain dissolved in the Al matrix [76].

The experimental AlSi9Cu3 alloy exhibited conductivity values within the typical range for aluminium casting alloys. In contrast, the Al80Mg10Si5Cu5 alloy presented a reduction of approximately 25 % in conductivity compared to AlSi9Cu3. This decline is directly related to the higher alloying element content in Al80Mg10Si5Cu5,

Despite this reduction, the conductivity remains comparable to other commercial aluminium alloys, indicating that the new alloy maintains an acceptable balance between conductivity and mechanical performance.

4.4.2. Density

The obtained density values confirm that the newly developed Al80Mg10Si5Cu5 alloy is significantly lighter than conventional HPDC aluminium alloys. This reduction is attributed to the careful selection of alloying elements and their proportions, which contributed to a weight decrease of approximately 10 % compared to the AlSi9Cu3 alloy.

These results are consistent with previous findings, where multicomponent aluminium alloys designed for lightweight applications have shown reduced density compared to standard alloys [26]. The lower density enhances the potential of this alloy for applications requiring weight reduction without compromising mechanical properties.

4.5. Mechanical properties

4.5.1. Hardness

The results indicate that the Al80Mg10Si5Cu5 alloy maintains its hardness more effectively at elevated temperatures compared to AlSi9Cu3. It could be explained by the sole presence of Al_2CuMg phases in the microstructure at 200 °C, with higher hardness values than the

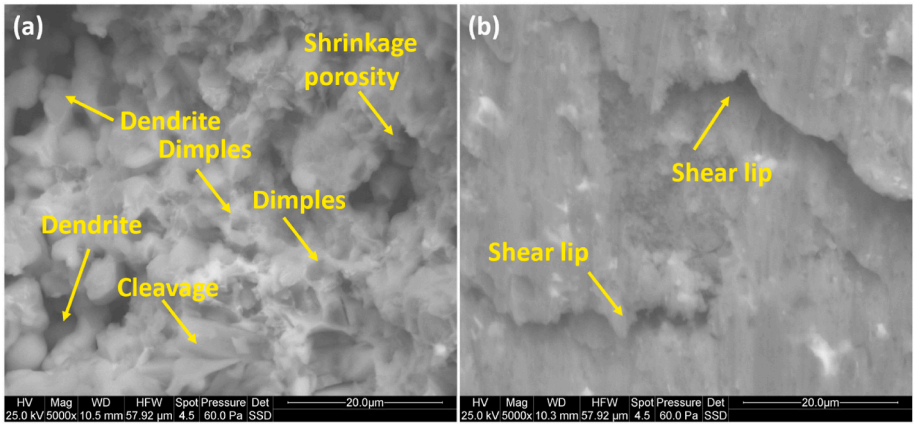

Fig. 17. x5000 SEM of compressive test specimens of Al80Mg10Si5Cu5 alloy (a) at RT; (b) at 200 °C.

Al_2Cu phase [17]. Moreover, the transformation of Al_2Cu to a more stable Al_2CuMg phase enhanced the retention of hardness and mechanical properties at elevated temperatures [17].

The obtained hardness values confirm that the Al80Mg10Si5Cu5 is about 40 % higher than AlSi9Cu3 alloy, with a well-known decrease of hardness values at 200 °C. This reinforces its suitability for applications requiring high mechanical performance at elevated temperatures.

4.5.2. Tensile strength

The improvement in mechanical strength is partially attributed to the hard reinforcement particles of polygonal and eutectic Mg_2Si, instead of coarse Mg_2Si particles that can act as stress concentration areas, promoting a decohesion at the particle-matrix interface and leading to crack initiation and propagation during deformation. This process weakens the materials reducing their capacity for plastic deformation, leading to a loss of ductility [95,96], by creating local stress concentration points at the interface, ultimately leading to crack initiation [83].

Moreover, as previously mentioned, the sole presence of Al_2CuMg phases in the 200 °C microstructure promotes higher strength and hardness values than the Al_2Cu phase [17]. This transformation enhances the retention of mechanical properties at elevated temperatures, making the Al80Mg10Si5Cu5 alloy more stable compared to conventional Al–Si–Cu alloys.

The Al80Mg10Si5Cu5 alloy showed similar values at RT and 200 °C, unlike the conventional aluminium alloys.

The HPDC process with rapid solidification resulted in a stable microstructure and mechanical properties [97]. The AlSi9Cu3 alloy is well known for its decrease in mechanical strength at temperatures higher than 150 °C. Despite demonstrating higher ductility than the studied alloy, this alloy is often characterized as near brittle at room temperature [41].

There is not a total consistency between the hardness tendency and the tensile properties in the Al80Mg10Si5Cu5 alloy. Normally, a decrease in hardness values promotes an increase in ductility and a decrease in strength. However, in this case, there is also a partial dissolution of the Mg_2Si particles in the FCC aluminium matrix in samples tested at 200 °C, and the Al_2Cu phase transforms into the Al_2CuMg phase. This combination can lead to a slight decrease in the hardness values with an increase of both ductility and strength.

It was observed that there was a slight dispersion in the obtained results. In HPDC, the distribution of defects can vary even when using the same parameters [98] leading to a higher dispersion in mechanical properties than in other metal-transforming processes.

To compare the YS of the Al80Mg10Si5Cu5 alloy with other aluminium alloys produced by HPDC and other processes [31,49,99,100], Fig. 18 presents a YS to density diagram. The Al80Mg10Si5Cu5 alloy exhibits an optimal balance between yield strength, tensile strength and density, and in the case of the alloys produced by HPDC the best values, especially at 200 °C. Although AlCuMnFeZr and AlCuMnFe alloys show comparable YS ratios and slightly higher UTS at RT, they are produced by casting processes different than HPDC, and experience a significant decrease in their properties at 200 °C.

Cracks can originate at the surface from manufacturing defects, though this was less common in HPDC samples [101]. The fracture mode of the as-cast Al80Mg10Si5Cu5 alloy showed a combination of ductile and brittle failure, with fragile fracture predominantly caused by the presence of primary Mg_2Si particles [46,85].

By implementing more efficient melting practices and optimizing component design, it is possible to reduce the occurrence of defects, thereby enhancing the overall strength of the casting [102].

4.5.3. Compressive strength

The increase in the compressive strength and reduced ductility of Al80Mg10Si5Cu5 at RT have been correlated with the presence of Mg_2Si phases. The compressive strength increases by raising the Mg_2Si concentration, contributing to a more brittle fracture behaviour [103]. The high deformation in AlSi9Cu3 may be attributed to its lower hardness.

The observed behaviour at 200 °C is typical in aluminium alloys, where softening occurs at temperatures above 150 °C, leading to an increase in deformation (D) and a decrease in UCS and YS [104]. However, in Al80Mg10Si5Cu5, an unusual slight increase in YS, which may be due to the transformation of the Al_2Cu to Al_2CuMg phase. This transformation has a significant effect on the comprehensive mechanical properties of the material [105].

The severe degradation of mechanical properties in AlSi9Cu3 at 200 °C, particularly the 40 % reduction in UCS, highlights the superior high-temperature stability of the Al80Mg10Si5Cu5 alloy.

It is confirmed, as in previous works [56] that defects typical of the HPDC process would have less influence in the compression test than in the tensile test, and some of them can be eliminated or decreased during the test.

To compare the compressive strength of the newly Al80Mg10Si5Cu5 alloy with other multi-component aluminium alloys reported in the literature, Fig. 19 presents a compressive strength to density diagram. The diagram includes the investigated AlSi9Cu3 alloy; multi-component aluminium alloys such as Al85Cu5Si5Zn5, Al65Cu10Mg10Si10Zn5, Al80Cu5Mg5Si5Zn5 [50], Al78Cu18Zn2Cr1Fe1, Al78Cu18Zn1Cr2Ti1 [23], as well as the Cantor alloys like CoCrFeMnNi [106] and Al0.5CoCrCuFeNi [107]. Additionally, a high-temperature aluminium alloy, AlSiCuMg with Zr, V, and Ti [108] is presented.

The newly developed Al80Mg10Si5Cu5 alloy, marked with a green colour in Fig. 19, demonstrates the best balance between density and compressive strength. While Cantor alloys show the highest values for UCS, they exhibit a significantly higher density of around 8 g/cm^3 with a lower strength to density ratio.

The fracture analysis provides further insight into the failure mechanisms of Al80Mg10Si5Cu5. The results are coherent with other studies,

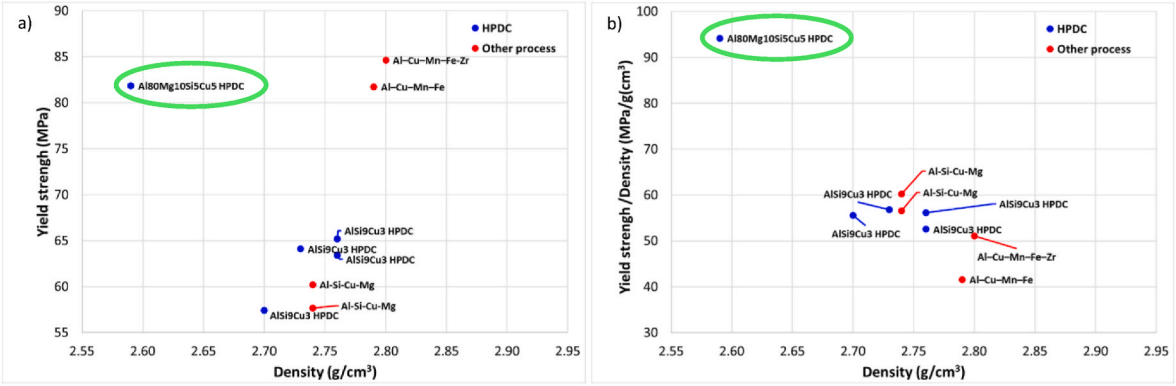

Fig. 18. Yield strength - density diagram, a) TA, b) 200 °C.

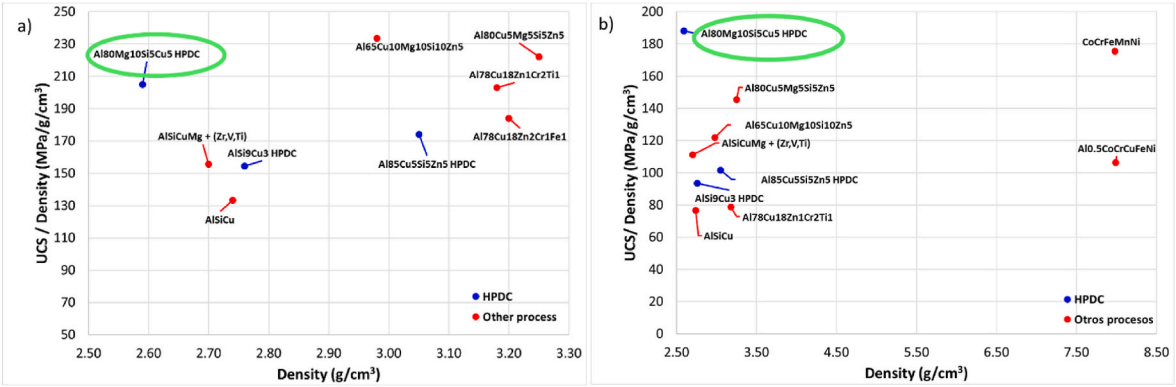

Fig. 19. Compressive strength - density diagram, a) TA, b) 200 °C.

where minor cracks initiated in the primary Mg_2Si particles promoted the fracture of these phases and propagated along the interdendritic and porous areas [103].

The fracture mode of the as-cast Al80Mg10Si5Cu5 alloy showed a combination of ductile and brittle failure, with a fragile fracture predominantly, in concordance with other similar alloys [85].

At 200 °C, the transition to a fully ductile fracture mode, with no visible cracks and extensive shear lips, confirms the enhanced plasticity at high temperatures. This behaviour is consistent with ductile fracture mechanisms reported in the literature [109]. Additionally, the fracture propagated at a 45-degree angle but involved a considerable plastic deformation of the sample before the fracture. This also justifies the greater ductility observed at high temperatures [110].

5. Conclusions

The main objective of this work was achieved: the development of a new as-cast multicomponent alloy with enhanced mechanical properties obtained by HPDC foundry process for heat applications.

The following conclusions can be drawn from the analysis.

- It was concluded that the mechanical properties of Al80Mg10Si5Cu5 alloy remained stable at temperatures up to 200 °C, demonstrating superior mechanical stability compared to AlSi9Cu3.
- A new HPDC casting alloy has been developed, exhibiting a superior YS, UTS, and UCS ratio.
- The alloy showed a refined surface layer which contributed to increase physical and mechanical properties. Avoiding the machining of HPDC cast parts could improve in-service performance under wearing conditions.
- The new as-cast Al80Mg10Si5Cu5 alloy was multiphase, with an FCC structure and Mg and Cu-rich phases with different constitutions which influenced its mechanical properties. While at RT the phase of Al_2CuMg was visible, at 200 °C it disappeared and transformed into Al_2Cu.
- The results of tensile tests indicated the development of a high-strength Al80Mg10Si5Cu5 alloy. The hardness and mechanical strength values exceeded those of other commercial aluminium alloys manufactured by HPDC foundry process at RT. At 200 °C, the mechanical properties remained stable, with yield strength and tensile strength being 65 % and 45 % higher than those of the AlSi9Cu3 alloy.
- The results of compressive tests indicated a good balance of compressive properties, combining high strength and deformation. Compared to AlSi9Cu3 alloy, the Al80Mg10Si5Cu5 alloy showed 40 % higher yield strength and 25 % higher ultimate compressive strength at RT, with deformation reduced by half. At 200 °C, the UCS only decreased by about 12 %, while the YS remained stable. Deformation also increased but remained at half the value of AlSi9Cu3. In contrast, the UCS of AlSi9Cu3 decreased by up to 40 % at 200 °C.
- The new alloy exhibited a density approximately 6 % lower than that of the AlSi9Cu3 alloy.
- The newly developed alloy shows promise as a cost-effective and low CO_2 alternative for aluminium drum brakes application. It offers advantages due to its performance properties obtained from secondary aluminium alloys, which are also lighter than iron, which potentially enhance fuel efficiency. Additionally, the HPDC process used for its production results in reduced cycle times among other advantages.

Future work will focus on studying new aluminium multicomponent alloys.

Declaration of competing interest

The authors declare the following financial interests/personal relationships which may be considered as potential competing interests: Joseba Albizuri reports financial support was provided from the Department of Industry, Energy Transition and Sustainability of the Basque Government (ELKARTEK Programme) and Universities (Call for Research Groups). Iban Vicario reports financial support was provided by Tecnalia Research & Innovation Foundation. Joseba Albizuri has patent #EP23383372.2 pending to UPV and Tecnalia. If there are other authors, they declare that they have no known competing financial interests or personal relationships that could have appeared to influence the work reported in this paper.

Acknowledgments

This work has been partially funded by the Basque Government through the ELKARTEK KK-2022/00082 (MINERVA), KK-2023/00020 (DESGAS) and IT1542-22.

References

[1] Lehmhus D. Advances in metal casting technology: a review of state of the art, challenges and trends—Part I: changing markets, changing products. Metals 2022;12:1959. https://doi.org/10.3390/met12111959.
[2] Dinesh PK, Darius S. Aluminium-Silicon based Metal Matrix Composites for brake rotor applications: a review. Eng Res Express 2023;5:2. https://doi.org/10.1088/2631-8695/accdb6.
[3] Dinberu B, Yoseph B. Investigation of mechanical and thermal properties of drum brake for light duty vehicle application. Int J Innovat Sci Eng Technol 2019;6:6.
[4] Applications – Chassis & Suspension – Brake system. The aluminium automotive manual. European-Aluminium Association; 2011. Available online: https://european-aluminium.eu/wp-content/uploads/2022/11/aam-applications-chassis-suspension-5-brake-system.pdf.
[5] Awe SA, Thomas A. The prospects of lightweight SICAlight discs in the emerging disc brake requirements. Eurobrake 2020:1–8.

[6] Yang H, Shouxun J, Yang W, Wang Y, fan Z. Effect of Mg level on the microstructure and mechanical properties of die-cast Al–Si–Cu alloys. Mater Sci Eng, A 2015;642:340–50. https://doi.org/10.1016/j.msea.2015.07.008.

[7] The Aluminium Automotive manual, European Aluminium Association, Available online: https://european-aluminium.eu/wp-content/uploads/2022/11/aam-products-6-cast-alloys-and-products.pdf.

[8] Bogdanoff T, Seifeddine S, dahle AK. The effect of Si content on microstructure and mechanical properties of Al-Si alloy. La Metall Ital 2016;108(6):65–9.

[9] Mehdi H. Effect of silicon content on the mechanical properties of aluminum alloy. Int Res J ENg Technol 2015;2(4):1326–30.

[10] Murugesan R, Venkataramana SH, Marimuthu S, Anand PB, Nagaraja S, Isaac JS, Sudharsan RR, Yunus TM, Almakayeel N, Islam S, Razak A. Influence of alloying materials Al, Cu, and Ca on microstructures, mechanical properties, and corrosion resistance of Mg alloys for industrial applications: a review. ACS Omega 2023;8(41):37641–53. https://doi.org/10.1021/acsomega.3c03417.

[11] Huang ZL, Kai W, Zhang ZM, Li B, Xue HS, Yang DZ. Effects of Mg content on primary Mg2 Si phase in hypereutectic Al−Si alloy. Trans Nonferrous Metals Soc China 2015;25(10):3197–203. https://doi.org/10.1016/S1003-6326(15)63956-5.

[12] Asghar G, Peng L, Fu P, Yuan L, Liu Y. Role of Mg_2Si precipitates size in determining the ductility of A357 cast alloy. Mater Des 2020;186:108280. https://doi.org/10.1016/j.matdes.2019.108280.

[13] Lisova L, Erber M, Fuchs G, Volk W, Rottenegger D, Braunreuther S. Dual-alloy sand mold casting: main principles and features. Int J Metalcast 2024. https://doi.org/10.1007/s40962-024-01289-6.

[14] Joseph OO, Olubambi PA, Joseph OO, Edun BM, Okeniyi JO, Abioye OP. Effects of alloying on aluminium-silicon alloys - a review. IOP Conf Ser Mater Sci Eng 2021;1107:012116. https://doi.org/10.1088/1757-899X/1107/1/012116.

[15] Monticelli C, Zanotto F, Balbo A, Grassi V, Fabrizi A, Timelli G. Corrosion behavior of high-pressure die-cast secondary AlSi9Cu3(Fe) alloy. Corros Sci 2022;209:110779. https://doi.org/10.1016/j.corsci.2022.110779.

[16] Kralik R, Battosova L, Kihoulou B, Preilser D, Cieslar M. High-temperature phase transformations in Al-Li-Cu-Mg-Zr-Sc alloy studied via in situ electron microscopy. Crystals 2024;14(2):136. https://doi.org/10.3390/cryst14020136.

[17] Zhang J, Huang YN, Mao C, Peng P. Structural, elastic, and electronic properties of θ (Al2Cu) and S (Al2CuMg) strengthening precipitates in Al–Cu–Mg series alloys: first-principles calculations. Solid State Commun 2012;152(23):2100–4. https://doi.org/10.1016/j.ssc.2012.09.003.

[18] Wen K, Yan H, Yan L, Liu H, Xiao W, Li Y, Gao G, Liu R, Ren W. Evolution of S (Al_2CuMg) phase during fabrication process and its influence on mechanical property in a commercial Al-6.5Zn-2.4Mg-2.2Cu alloy. In: Advances in machinery. Materials science and engineering application IX. Amsterdam, The Netherlands: IOS Press; 2023. p. 155–65. https://doi.org/10.3233/ATDE230454.

[19] Kumar J, Jha S, Raturi A, Bajpai A, Sonkusare R, Gurao NP, Biswas K. Novel alloy design concepts enabling enhanced mechanical properties of high entropy alloys. Front Mater 2022;9:868721. https://doi.org/10.3389/fmats.2022.868721.

[20] Balaji V, X Anthony. Development of high entropy alloys (HEAs): current trends. Heliyon 2024;10:e26464. https://doi.org/10.1016/j.heliyon.2024.e26464.

[21] Bilbao Y, Trujillo JJ, Vicario I, Arruebarrena G, Hurtado I, Guraya T. X-Ray thermo-diffraction study of the aluminum-based multicomponent alloy Al58Zn28Si8Mg6. Materials 2022;15:5056. https://doi.org/10.3390/ma15145056.

[22] He JY, Liu WH, Wang H. Effects of Al addition on structural evolution and tensile properties of the FeCoNiCrMn high-entropy alloy system. Acta Mater 2014;62(1):105. https://doi.org/10.1016/j.actamat.2013.09.037.

[23] Cui L, Zhang Z, Chen XG. Development of lightweight Al-based entropy alloys for elevated temperature applications. J Alloys Compd 2022;938(4):168619. https://doi.org/10.1016/j.jallcom.2022.168619.

[24] Yang X, Chen S, Cotton JD, Zhang Y. Phase stability of low-density, multiprincipal component alloys containing aluminium, magnesium, and lithium. J Miner Met Mater Soc 2014;66:2009. https://doi.org/10.1007/s11837-014-1059-z.

[25] Sanchez JM, Vicario I, Albizuri J, Guraya T, Koval NE, García JC. Compound formation and microstructure of As-cast high entropy aluminiums. Metals 2018;8:167. https://doi.org/10.3390/met8030167.

[26] Kumar A, Gupta M. An insight into evolution of light weight high entropy alloys: a review. Metals 2016;6:199. https://doi.org/10.3390/met6090199.

[27] Sheikh S. Alloy design for high-entropy alloys: predicting solid solubility, and balancing mechanical properties and oxidation resistance. Mater Sci Eng 2018. Thesis Chalmers University of Technology (Sweden), Available online: https://research.chalmers.se/publication/503532/file/503532_Fulltext.pdf.

[28] Sanchez JM, Pascual A, Vicario I, Albizuri J, Guraya T, Galarraga H. Microstructure and phase formation of novel Al80Mg5Sn5Zn5X5 light-weight complex concentrated aluminum alloys. Metals 2021;11(2):1944. https://doi.org/10.3390/met11121944.

[29] Sanchez JM, Vicario I, Albizuri J, Guraya T, Acuña EM. Design, microstructure and mechanical properties of cast medium entropy aluminium alloys. Sci Rep 2019;9(1):6792. https://doi.org/10.1038/s41598-019-43329-w.

[30] Zhang B, Liaw PK, Brechtl J, Ren J, Guo X. Effects of Cu and Zn on microstructures and mechanical behavior of the medium-entropy aluminum alloy. J Alloys Compd 2019:153092. https://doi.org/10.1016/j.jallcom.2019.153092.

[31] Sanchez JM. Propiedades tribológicas y de fatiga de nuevas aleaciones de aluminio basadas en el concepto de alta entropía. Mech Eng 2021. University of the Basque Country, Spain.

[32] Sanchez JM, Vicario I, Albizuri J, Guraya T, García JC. Phase prediction, microstructure and high hardness of novel light-weight high entropy alloys. J Mater Res Technol 2019;8(1):795–803. https://doi.org/10.1016/j.jmrt.2018.06.010.

[33] Nunes H, Emadinia O, Vierira MF, Reis A. Low- and high-pressure casting aluminum alloys: a review, recent advancements in aluminum alloys. Recent Adv Alum Alloy 2024:1–19. https://doi.org/10.5772/intechopen.109869.

[34] Otarawanna S, Gourlay C, Laukli HI, Dahle AK. Formation of the surface layer in hypoeutectic Al-alloy high-pressure die castings. Mater Chem Phys 2011;130(1):251. https://doi.org/10.1016/j.matchemphys.2011.06.035.

[35] Tialong Z, Zhu J, yang T, Luan J, Kong HL, Liu W, Cao B, Wu S, Wang D, Wang Y, Liu CT. A new $\alpha + \beta$ Ti-alloy with refined microstructures and enhanced mechanical properties in the as-cast state. Scr Mater 2022;207:114260. https://doi.org/10.1016/j.scriptamat.2021.114260.

[36] Palyga L, Stachowicz M, Granat K. Influence of high-pressure die-casting second stage parameter on structure of AlSi9Cu3(Fe) alloy. Manuf Technol 2016;16(2):410. https://doi.org/10.21062/ujep/x.2016/a/1213-2489/MT/16/2/410.

[37] Fan KL, Liu XS, He GQ, Chen H. Elevated temperature low cycle fatigue of a gravity casting Al–Si–Cu alloy used for engine cylinder heads. Mater Sci Eng, A 2015;632(24):127–36. https://doi.org/10.1016/j.msea.2015.02.069.

[38] Závodská D, Tillová E, Svecová I, Chalupová M, Kucharíková L, Belan J. The effect of iron content on microstructure and porosity of secondary AlSi7Mg0.3 cast alloy. Period Polytech Transp Eng 2018;47:4. https://doi.org/10.3311/PPtr.12101.

[39] Zovko Z, Dolic N, Unkic F. Influence of copper content on microstructure development of AlSi9Cu3 alloy. J Min Metall B Metall 2014;50(1):53. https://doi.org/10.2298/JMMB130125009B.

[40] Bolibruchova D, Podprocka R, Pastircak R, Major-Gabrys K. The role of Mn in aluminium alloys with a higher iron content. Arch Metall Mater 2018;63(4):1883–8. https://doi.org/10.24425/amm.2018.125119.

[41] Gain S, Silva TEF, Jesus AMP, Cavaleiro A, Rosa PAR, Reis A. Mechanical characterization of the AlSi9Cu3 cast alloy under distinct stress states and thermal condition. Eng Fract Mech 2019;216:106499. https://doi.org/10.1016/j.engfracmech.2019.106499.

[42] Lehmhus D, Rahn T, Struss A, Gromzig P, Wischeropp T, Becker H. High-temperature mechanical properties of stress-relieved AlSi10Mg produced via laser powder bed fusion additive manufacturing. Materials 2022;15(20):7386. https://doi.org/10.3390/ma15207386.

[43] MRT castings. Available online: https://www.mrt-castings.co.uk/aluminium-die-casting-alloys-lm9.html.

[44] Lee JA. Cast aluminum alloy for high temperature applications. The Minerals. Metal Soc 2003.

[45] Shuiqiang Z, Zhang Y, Chen M, Wang Y, Cui Q, Wu E, Arola D, Zhang D. Characterization of mechanical properties of aluminum cast alloy at elevated temperature. Appl Math Mech 2018;39(7):967–80. https://doi.org/10.1007/s10483-018-2349-8.

[46] Mohamed AMA, Samuel F, Al Kahtani S. Microstructure, tensile properties and fracture behavior of high temperature Al–Si–Mg–Cu cast alloy. Mater Sci Eng 2013;577:64–72. https://doi.org/10.1016/j.msea.2013.03.084.

[47] Zamani M, Seifeddine S, Jarfors AEW. High temperature tensile deformation behavior and failure mechanisms of an Al-Si-Cu-Mg cast alloy - the microstructural scale effect. Mater Des 2015;86(5):361–70. https://doi.org/10.1016/j.matdes.2015.07.084.

[48] Timelli G, Fabrizi A, Vezzù S, De Mori A. Design of wear-resistant diecast AlSi9Cu3(Fe) alloys for high-temperature components. Metals 2019;10(1):55. https://doi.org/10.3390/met10010055.

[49] Garibaldi E, Lemke JN, Rovatti L, Baer O, Timelli G, Bonollo F. High-temperature behavior of high-pressure diecast alloys based on the Al-Si-Cu system: the role played by chemical composition. Metals 2018;8(5):348. https://doi.org/10.3390/met8050348.

[50] Sanchez JM, Galarraga H, Del Molino E, Albizuri J, Guraya T, Hudson SW. Microstructure and mechanical properties of two novel scrap tolerant Al65Cu10Mg10Si10Zn5 and Al80Cu5Mg5Si5Zn5 high entropy aluminum alloys. Intermetallics 2023;162:108023. https://doi.org/10.1016/j.intermet.2023.108023.

[51] Development-of-high-strength-multicomponent-aluminium-based-die-casting-alloy. Available online:http://static1.squarespace.com/static/5f9038b94479af49c908d45c/5f903967a27c1d3e0d7d8ad2/5f903965a27c1d3e0d7d8907/1603287397631/Development-of-high-strength-multicomponent-aluminium-based-die-casting-alloys.pdf?format=original.

[52] Shao Y, Guo P, Liang N, Cheng S, Wang J, Xu F. Microstructure refinement and enhanced mechanical properties in rapid-quenched MnCrFeCoNi high-entropy alloy. Heliyon 2023;9(12):e22530. https://doi.org/10.1016/j.heliyon.2023.e22530.

[53] Tun KS, Murugan P, Srivatsan TS, Gupta M. Synthesis and Characterization of aluminium based multicomponent alloys. Mater Today Proc 2021;46(2):1210. https://doi.org/10.1016/j.matpr.2021.02.066.

[54] Sanna F, Fabrizi A, Ferraro S, Timelli G, Ferro P, Bonollo F. Multiscale characterisation of AlSi9Cu3(Fe) die casting alloys after Cu, Mg, Zn and Sr addition. La Metall Ital 2013;15(4):13.

[55] Zbontar M, Petric M, Mrvar P. The influence of cooling rate on microstructure and mechanical properties of AlSi9Cu3. Metals 2021;11(2):186. https://doi.org/10.3390/met11020186.

[56] Gu C, Lu Y, Luo A. Three-dimensional visualization and quantification of microporosity in aluminum castings by X-ray micro-computed tomography. J Mater Sci Technol 2020;65:99. https://doi.org/10.1016/j.jmst.2020.03.088.

[57] Djurdjevic MB. Application of thermal analysis in ferrous and non-ferrous foundries. J Inst Eng 2021;27:457–71. https://doi.org/10.30544/673.

[58] Djurdjevic MB, Vicario I, Huber G. Review of thermal analysis applications in aluminium casting plants. Rev Metal (Madr) 2013;50(1):e004. https://doi.org/10.3989/revmetalm.004.
[59] Sparkman D. Micro event analysis of cooling curves. Meltlab Syst 2019. Available online: https://meltlab.com/.
[60] Yi W, Gao J, Zhang L. A CALPHAD thermodynamic model for multicomponent alloys under pressure and its application in pressurized solidified Al–Si–Mg alloys. Adv Powder Mater 2024;3(3):100182. https://doi.org/10.1016/j.apmate.2024.100182.
[61] Villanueva E, Vicario I, Sanchez JM, Crespo I, Albizuri J, Guraya T, Análisis térmico diferencial aplicado en la investigación de las aleaciones Al80Mg5Sn5Zn5Ni5 y Al80Mg5Sn5Zn5Ti5, CNMAT congress 2022 (Spain).
[62] Nandhakumar S, Santhkumar WE, Shunmughanaathan Vk. Experimental analysis of aluminium matrix composite material for braking application. Mater Today Proc 2020;37(8–9). https://doi.org/10.1016/j.matpr.2020.08.375.
[63] Das S, Siddiqui AR, Bartaria V. Evaluation of aluminum alloy brake drum for automobile application. Int J Sci Technol Res 2013;2(11):96–102.
[64] Vicario I, Anza I, Saenz De Tejada F, García JC, Galarraga H, Merchan M. Development of new Al-Si9Cu3 alloys for HPDC components with tailored properties. In: 71st World foundry congress: advanced sustainable foundry; 2014. Bilbao, Spain.
[65] Vander GF, Fowler R, Low-Load Vickers Microindentation, Royal Belgian Institute of Marine Engineers. Available online: https://www.gallois.be/ggmagazine_2012/gg_06_11_2012_280.pdf.
[66] Tebib M, Ajersh F, Samuel AM, Chen XG. Solidification and microstructural evolution of hypereutectic Al-15Si-4Cu-Mg alloys with high magnesium contents. Metall Mater Trans 2013;44(9):4281–95. https://doi.org/10.1007/s11661-013-1769-9.
[67] Voncina M, Kores S, Mrvar P, Medved J. Effect of Ce on solidification and mechanical properties of A360 alloy. J Alloys Compd 2011;509(27):7349. https://doi.org/10.1016/j.jallcom.2011.04.059.
[68] Shengli Y, Shen J, Xiaodong Y, Xiwu L, Fei Z, Baoqing S. Homogenization treatment parameter optimization and microstructural evolution of Al-Cu-Li alloy. Rare Met Mater Eng 2017;46(1):28. https://doi.org/10.1016/S1875-5372(17)30072-3.
[69] Samuel E, Samuel AM, Songmene V, Samuel FH. A review on the analysis of thermal and thermodynamic aspects of grain refinement of aluminum-silicon-based alloys. Materials 2023;16(6):5639. https://doi.org/10.3390/ma16165639.
[70] Yang H, Watson D, Wang Y, Shouxun J. Effect of nickel on the microstructure and mechanical property of die-cast Al–Mg–Si–Mn alloy. J Mater Sci 2014;49:8412–22. https://doi.org/10.1007/s10853-014-8551-2.
[71] Vijayan V, Narayan K. Review of microstructure evolution in hypereutectic Al–Si alloys and its effect on wear properties. Trans Indian Inst Met 2014;67(1):1–18. https://doi.org/10.1007/s12666-013-0327-x.
[72] Belov NA, Avksenteva NN. Quantitative analysis of the Al –Cu –Mg – Mn – Si phase diagram as applied to commercial aluminum alloys of series 2xxx. Met Sci Heat Treat 2013;55(7):358–63. https://doi.org/10.1007/s11041-013-9635-3.
[73] Mondal C, Mukhopadhyay AK. On the nature of T(Al2Mg3Zn3) and S(Al2CuMg) phases present in as-cast and annealed 7055 aluminum alloy. Mater Sci Eng, A 2005;391(1–2):367. https://doi.org/10.1016/j.msea.2004.09.013.
[74] Taylor JA. Iron-containing intermetallic phases in Al-Si based casting alloys. Proc Mater Sci 2012;1:19–33. https://doi.org/10.1016/j.mspro.2012.06.004.
[75] Liu Y, Xiong S. Research progress on thermal conductivity of high-pressure die-cast aluminum alloys. Metals 2024;14:370. https://doi.org/10.3390/met14040370.
[76] Liu Y, Zhang Y, Liu W, Jiao X, Nishat H, Ajavavarakula D, Chen H, Xiong S. Enhanced mechanical properties and thermal conductivity of high-pressure die-cast AlMg6Si2MnZr alloy by controlling the externally solidified crystals. J Mater Process Technol 2022:117645. https://doi.org/10.1016/j.jmatprotec.2022.117645.
[77] Li Y, Hu A, Fu Y, Liu S, Shen W, Hu H, Nie X. Al alloys and casting processes for induction motor applications in battery-powered electric vehicles: a review. Metals 2022;12(2):216. https://doi.org/10.3390/met12020216.
[78] Yang Z, he X, Li B, Atrens A, Yang X, Cheng H. Influence of Si, Cu, B, and trace alloying elements on the conductivity of the Al-Si-Cu alloy. Materials 2022;15(2):426. https://doi.org/10.3390/ma15020426.
[79] Electrical Conductivity and Resistivity for Aluminum and Aluminum Alloys, Iowa State University. Available online: https://www.nde-ed.org/NDETechniques/EddyCurrent/ET_Tables/ET_matlprop_Aluminum.xhtml.
[80] European Steel and alloys grades. Available online: http://www.steelnumber.com/en/steel_alloy_composition_eu.php?name_id=1224.
[81] Aluminum alloy ALSI9CU3. Available online: https://www.sunrise-metal.com/aluminum-alloy-alsi9cu3.
[82] NADCA product specification standards for die casting. In: Die casting handbook. NADCA. Nadca publication #G200; 2015.
[83] Gowda KP, Prakash JN, Gowda S, Boppana SB. Effect of particulate reinforcement on the mechanical properties of Al2024-WC MMCs. J Miner Mater Char Eng 2014;3(6):469–76. https://doi.org/10.4236/jmmce.2015.36049.
[84] Tarafder S, Ranganath VR, Sivaprasad S, Johri P. Ductile fracture behaviour of primary heat transport piping material of nuclear reactors. Sadhana 2003;28(1):167–86. https://doi.org/10.1007/BF02717132.
[85] Warmuzek M. Aluminum-silicon casting alloys, atlas of microfractographs, vol. 14. ASM International; 2004.
[86] Zhang GH, Zhang JX, Li BC, Cai W. Characterization of tensile fracture in heavily alloyed Al–Si piston alloy. Prog Nat Sci 2011;21(5):380–5. https://doi.org/10.1016/S1002-0071(12)60073-2.
[87] Jiao XY, Wang J, Liu CF, Guo Z, Tong GD, Ma SL, Bi Y, Zhang YF, Xiong S. Characterization of high-pressure die-cast hypereutectic Al-Si alloys based on microstructural distribution and fracture morphology. J Mar Sci Technol 2018. https://doi.org/10.1016/j.jmst.2018.12.005.
[88] Aluminum 356.0-T7, Permanent Mold Cast, Matweb. Available online: http s://www.matweb.com/search/datasheet_print.aspx?matguid=408de34dab50434f995379fda4cf97f7.
[89] Kumar S, Czerwinski F, Kasprzak W, Chen D. Tensile and compressive deformation behavior of the Al-Si-Cu-Mg cast alloy with additions of Zr, V and Ti. Mater Des 2014;9:352. https://doi.org/10.1016/j.matdes.2014.02.060.
[90] Smirnov S, Vichuzhanin D, Nesterenko A, Smirnov A, Pugacheva N, Konovalov A. A fracture locus for a 50 volume-percent Al/SiC metal matrix composite at high temperature. Int J Material Form 2017;10:5. https://doi.org/10.1007/s12289-016-1323-6.
[91] Zuidema J, Veer F, Van Kranenburg C. Shear lips on fatigue fractures in aluminium alloy sheet material. Fatig Fract Eng Mater Struct 2004;28(1–2):159. https://doi.org/10.1111/j.1460-2695.2004.00837.x.
[92] Effect of iron on the microstructure and mechanical property of Al–Mg–Si–Mn and Al–Mg–Si diecast alloys.
[93] Schweizer P, Sharma A, petho L, Huszar E, Vogl LM, Michler J, Maeder X. Atomic scale volume and grain boundary diffusion elucidated by in situ STEM. Nat Commun 2023;14(1):7601. https://doi.org/10.1038/s41467-023-43103-7.
[94] Mackenzie S. Heat treatment of aluminum Part VII - hardness and conductivity. Thermal Proc 2021.
[95] Shafieizad AH, Zarei-Hanzaki A, Abedi HR, Al-Fadhalah KJ. The Mg2Si phase evolution during thermomechanical processing of in-situ aluminium matrix macro-composite. Mater Sci Eng 2015;664:310–7. https://doi.org/10.1016/j.msea.2015.07.060.
[96] Wu X, Zhao F, Wu F, Jikang Q. Development of a near eutectic Al-Mg 2 Si-Mg alloy with high strength and toughness. J Mater Eng Perform 2024. https://doi.org/10.1007/s11665-024-09789-6.
[97] Czerwinski F. Thermal stability of aluminum alloys. Materials 2020;13(15):3441. https://doi.org/10.3390/ma13153441.
[98] Timelli G, Bonollo F, Cupito G. The impact of defects on the quality of aluminium alloy die castings. ATA-Ingegneria dell Àutoveicolo 2009;62:12–9.
[99] Zamani M, Seifeddine S, Jarfors AEW. High temperature tensile deformation behavior and failure AlSiCuMg cast alloy-the microstructural scale effect. Mater Des 2015:135564246. https://doi.org/10.1016/j.matdes.2015.07.084.
[100] Liu J, Hu J, Li M, Liu G, Wy Y, Gao T, Liu S, Liu X. Influence of Zr microalloying on the microstructure and room-/high-temperature mechanical properties of an Al–Cu–Mn–Fe alloy. Materials 2024;17(9):1–16. https://doi.org/10.3390/ma17092022.
[101] Noorian A, Fatemi A. Fatigue design with high pressure die cast aluminum including the effects of defects, section size, stress gradient, and mean stress. Mater Today Commun 2021:101567. https://doi.org/10.1016/j.mtcomm.2020.101567.
[102] Bonollo F, Gramegna N, Timelli G. High-pressure die-casting: contradictions and challenges. J Occup Med 2015;67:901–8. https://doi.org/10.1007/s11837-015-1333-8.
[103] Biswas P, Mandal D, Mondal MK. Compressive failure analysis of in-situ Al-Mg2Si composites: experiment and finite element modelling. Eng Fract Mech 2022;277:108986. https://doi.org/10.1016/j.engfracmech.2022.108986. 9-109.
[104] Kiefel A, Gimmler S, Broeckmann C, Vroomen U. Zn-based alloys for plain bearings—influence of Al and Cu content on mechanical properties. Materials 2024;17(5):1062. https://doi.org/10.3390/ma17051062.
[105] Fang X, Li Y, Zheng Q, Guo J, Yang Y, Ding W, Ma C, He K, Su N, Jiang J, Chen X, Wang H. Theoretical prediction of structural, mechanical, and thermophysical properties of the precipitates in 2xxx series aluminum alloy. Metals 2022;12(12):2178. https://doi.org/10.3390/met12122178.
[106] Kim YK, Yang S, Lee KA. Superior temperature-dependent mechanical properties and deformation behavior of equiatomic CoCrFeMnNi high-entropy alloy additively manufactured by selective laser melting. Sci Rep 2020;10:8045. https://doi.org/10.1038/s41598-020-65073-2.
[107] Diao H, Xie X, Sun F, Dahmen KA, Liaw PK. Mechanical properties of high-entropy alloys. Springer; 2016. p. 181–236. https://doi.org/10.1007/978-3-319-27013-5_6. High-Entropy Alloys.
[108] Czerwinski F, Kasprzak W, Sediako DG, Emadi D, Kumar S, Friedman J, chen D. Development of high temperature aluminum alloys for automotive powertrain. AM&P Tech Article 2016;174(3):16–20. https://doi.org/10.1007/s11837-015-1333-8.
[109] Azmeer M, Azhar M. Effect of side groove on shear lips formation of aluminium alloy 6061 using finite element analysis. J Adv Mech Eng Appl 2021;2(1):41. https://doi.org/10.30880/jamea.2021.02.01.005.
[110] Mouritz AP. Fracture processes of aerospace materials. Introd Aero Mater 2012;18:428.

Joseba Albizuri Irigoyen: Industrial Engineer from the University of the Basque Country (UPV/EHU) in 1990, where he also obtained his PhD in Industrial Engineering in 1994. Since 1990, he has served as a professor at UPV/EHU. Troughout his academic career, he has taught a wide range of subjects, including Algebra, Differential Equations, Classical Mechanics, Machine Construction and Testing, Finite Element Analysis, CAE Design, and Experimental Modal Analysis. His research focuses on finite element methods, experimental modal analysis, fatigue design of metallic components, and the mechanical engineering of advanced materials. Over the years, he has supervised 9 doctoral theses, primarily in the areas of material fatigue, the development of new alloys and advanced materials, numerical modeling, and the optimization of manufacturing processes. Joseba

has been actively involved in numerous research projects, contributing to the advancement of knowledge in his field. He has authored or co-authored approximately 50 scientific publications in high-impact journals and has conducted around 100 peer reviews for 11 different scientific publications, underscoring his role as a recognized expert in his discipline.

Teresa Guraya Diez: Degree in Chemical Sciences from the University of the Basque Country (UPV/EHU) and a PhD in Physical Sciences from the University of Navarra in 1995. She completed her doctoral studies in the Materials Department at the Gipuzkoa Center for Technical Research (Ceit-IK4). Currently, she is a professor in the Department of Mining and Metallurgical Engineering and Materials Science at UPV/EHU. Throughout her career, she has undertaken research stays at prestigious institutions, including Drexel University, Stanford University, Queen Mary University of London, the University of Malta, and Auckland University of Technology. Her current research focuses on exploring the relationships between physical metallurgy and the development of high value-added metallic alloys. Teresa actively collaborates with companies and research centers in the metallurgical sector through projects ranging from fundamental research to those with high industrial impact. She has contributed to over 30 scientific publications and is a member of The Minerals, Metals & Materials Society (TMS) and the Spanish Society of Materials (SOCIEMAT).

Iñaki Hurtado Hurtado: Graduated in Physical Sciences from UPV (1986), Master's and PhD in Materials Engineering from the Catholic University of Leuven (1994), and "Marie Curie Fellow" at RWTH Aachen. He has interdisciplinary training in alloy design through thermodynamic modeling and various experimental techniques. Since 2001, he has been a professor at the Faculty of Engineering at Mondragon Unibertsitatea, teaching courses in Materials and Processes. His research activities also focus on these fields, supervising doctoral theses on Aluminum alloys (semisolid forming), Magnesium (aerospace alloys), Casting (process improvement), and Electromagnetic Forming, among other topics. These projects are supported by funding from both public administrations and private companies, including the coordination of the Strategic Singular Project IntegrAuto (2008–2011). He is the author of approximately 30 articles in indexed journals, editor of four books, and has presented about 50 works at National and International Conferences.

Iban Vicario Gomez: Graduated in Mechanical Engineering in 1995 and Materials Engineering in 2004 from the University of the Basque Country. He also earned a Master's degree in Production Management from Mondragon University (1997), and a PhD in Condensed Matter Chemistry from the University of Bordeaux I (2011). Since 2007, he has worked at Tecnalia, where he is currently serves as a Project Director in the Foundry and Metallurgy Department. His work focuses on the research and development of innovative metallic materials and their manufacturing processes, the development of advanced alloys, and the recovery of metals from complex materials. Iban is the principal inventor of 8 European patents: He has led over 30 national and international projects, contributing significantly to advancements in metallurgical science and technology. In recognition of his achievements, he has awarded the prize for the best scientific presentation at the World Foundry Congress (WFC) in 2018.

Iñigo Crespo Camino: Industrial Technical Engineer from the he University of the Basque Country (UPV/EHU) in 1997. He began his professional career as a trainee at INASMET until 2001, when he joined TECNALIA, where he has remained a key contributor in the Foundry and Advanced Materials Department. From 2002 to 2007, he served as Head of the Foundry Center, overseeing various strategic initiatives and technological advancements. Over the years, he has actively participated in numerous R&D projects at the local, national, and European levels. His core expertise includes the development of advanced alloys for high-performance applications, the study of materials and manufacturing processes for continuous casting moulds, and the design of innovative thermal treatments aimed at enhancing productivity. Through his contributions, Iñigo has played a pivotal role in advancing metallurgical science and industrial applications.

Ester Villanueva Viteri: Technical Engineer in General Chemistry, specializing in Metallurgical (2012), Master's in Advanced Materials Engineering (2015–2017), and currently pursuing a PhD in Mechanical Engineering, all from the University of the Basque Country (UPV/EHU). Since 2014, she has been a researcher at TECNALIA, working in the Foundry and Metallurgy area. Her research expertise spans the development of innovative metallic alloys, process and treatment optimization, materials recovery and regeneration, and the application of advanced analytical techniques. She has been involved in over 22 national and European R&D projects and has presented her work at prominent conferences, including the National Materials Conference (CNMAT 2022 and CNMAT 2024) and EUROCORR 2023. Ester's contributions reflect her dedication to advancing materials science and industrial applications.